Review

Computation-Guided Support to Experiments by the Exploration of Reaction Mechanisms: Organic Synthesis, Natural Products and Environmental Issues

Karine N. de Andrade, [*,a] *José Renato D. Fajardo,* [b] *Caio A. Leal,* [a]
José Walkimar M. Carneiro [b] *and Rodolfo G. Fiorot* [*,a]

*aDepartamento de Química Orgânica, Instituto de Química, Universidade Federal Fluminense,
24020-141 Niterói-RJ, Brazil*

*bDepartamento de Química Inorgânica, Instituto de Química, Universidade Federal Fluminense,
24020-141 Niterói-RJ, Brazil*

Humankind has experienced a remarkable development since it began to design and optimize chemical reactions to achieve valuable compounds. The key to accomplish these tasks is the proper understanding of how chemical transformations occur at a molecular level, that is, their reaction mechanisms. Based on a suitable mechanistic proposal, experimentalists choose a given chemical protocol to optimize experimental conditions, design new synthetic routes, and circumvent competing reactions. In this context, computational chemistry has become a valuable ally for mechanistic elucidation. We present herein a review of complementary collaborations between experimentalists and theoretical chemists to rationalize processes at the molecular level, focusing mainly on the fields of organic synthesis, natural product chemistry, and systems with environmental interest. Throughout this review, we highlight the ability of computational evaluations to provide answers to questions raised from experiments in a clear and direct way, indicating to experimentalists alternative paths to help them solve their problems.

Keywords: computational chemistry, DFT, molecular modeling, reaction mechanism, reaction pathways

1. Introduction

One of the main objectives of chemists is to master the transformations of the matter. Since it was realized that it is possible to mimic the nature in producing chemical substances, e.g., the seminal work of Friedrich Wöhler, who in 1828 synthesized urea (a naturally occurring substance from living beings) from mineral reactants in laboratory,[1] and even to create highly specific molecules with desirable properties, humankind has experienced a remarkable development. Since then, efforts have been devoted to design and optimize chemical routes to achieve valuable substances by means of efficient and sustainable protocols. The knowledge about how chemical reactions occur at the molecular level, that is, their mechanisms, and what are the features that control reactivity is the key to accomplish these tasks.

The IUPAC Gold Book[2] defines the reaction mechanism as a meticulous description of the process converting reactants to products. It should inform in detail the composition, structure, relative energy of transition states and chemical intermediates and other properties. In addition, the hypothesized mechanism must be consistent with experimental evidence, such as stoichiometry, rate law, stereochemical aspects of intermediates and products and be compatible with any available experimental data. Deciphering a reaction mechanism requires the puzzling task of gathering a plethora of matching information and combine them to build a reasonable model. However, a famous quote attributed to Einstein in a biochemistry textbook concerning enzymatic mechanistic discussion states that "No amount of experimentation can ever prove me right; a single experiment can prove me wrong".[3] In another quotation, as found in many popular Organic Chemistry textbooks from undergraduate students to specialized audience, a reaction mechanism can never really be proven, once one single evidence can rule out a mechanistic model.[4-6] This is a controversial topic and literature presents warming debates.[7,8]

*e-mail: karineandrade@id.uff.br; rodolfofiorot@id.uff.br
Editor handled this article: Paula Homem-de-Mello (Associate)

Despite all this philosophical discussion about the provability of reaction mechanisms, we should be able to create reasonable models to understand and predict chemical phenomena based on the collected evidences. Notwithstanding, obtaining all the experimental data is laborious. In some cases, there are severe instrumental and operational limitations that makes elucidation of reaction mechanism solely based on experimental evidence almost prohibitive. In this context, computational chemistry stands as a powerful tool that can be employed to help facing these problems by simulating chemical and physical processes, in particular to access thermodynamic and kinetic parameters for the reaction of interest. The advance in computer technology has established this area as one of the three main cornerstones to chemical sciences, alongside with synthesis and spectroscopy.[9] In addition of their usefulness in the study of chemical reactions, computational tools have found their way in the simulation of several types of spectra (infrared (IR), nuclear magnetic resonance (NMR), UV-Vis, and Raman), which can be compared with those obtained from experiment,[10] helping elucidate the nature of elusive species, such as reaction intermediates. The computation of energetic parameters of a chemical reaction allows to evaluate its feasibility from the thermochemical (e.g., shifting of chemical equilibria, relative stability, acidity, basicity) or kinetic point of view (e.g., reaction rates and kinetic isotope effect).[11-15]

Computational chemistry explores the central concept of Potential Energy Surfaces (PES) to evaluate reaction mechanisms.[16] These are defined as hypersurfaces that express the correlation between the nuclear configurational arrangement of a given system (such as interatomic distance, r, valence angle, θ, and dihedral angles ϕ) and its corresponding potential energy, E_p. When the nuclear configuration is expressed in terms of the internal coordinates (q_i), according to their degree of freedom, the potential energy, E_p, becomes a function of those internal coordinates, $E_p = f(q_i)$.[17]

To compute the energy and the properties of a chemical system (a single molecule or an arrangement of substances in a chemical reaction), many computational models based on the classical or quantum laws of physics are available. Since chemical reactions involve bond forming/bond breaking events, the computational methods must invoke the quantum laws of physics to properly deal with the electron reorganization phenomena. Some of the commonly available models based on quantum mechanics are the Hartree-Fock (HF) method,[18] the Generalized Valence Bond Theory (GVBT),[19,20] Configuration Interaction (CI) methods,[21,22] Multi-Reference Configuration Interaction (MRCI),[23,24] Complete Active Space Perturbation Theory

(CASPT)[25,26] and Density Functional Theory (DFT).[17,27-29] The choice for a given method should consider the computational cost and the level of accuracy required for the calculated parameters. Because of the intricate quantum behavior of electrons and the algebraic treatment behind the formulations, many approximations are applied to enable their practical usage in computational research. One of the most fundamental is the Born-Oppenheimer (BO) approximation, which decouples the electronic and nuclear motions and treats them as independent from each other. The validity of the BO approximation arises from the fact that, for most cases, the electrons move much faster than the nuclei, due the high difference in their relative masses. Therefore, one can assume that electrons may instantly reorganize with respect to the nuclear motion. The assumption of the BO approximation allows the construction of the PESs.[16]

A point that may be crucial when studying reaction mechanisms is the consideration of dispersive forces in systems where non-covalent interactions are relevant. While these interactions are negligible for small systems, they may become critical for large ones. Dispersive interactions (or London dispersion forces) are quantum effects that arise from the correlation in the electron motion.[30] They are weak and strongly dependent on the distance between the interacting atoms.[31-33] The proper simulation of the dispersive forces is important in the design of molecules with unexpected long C–C bonds[34-36] and in the control of reactivity and selectivity in reactions with bulk components.[37-39] Although highly accurate methods (e.g., post-Hartree-Fock methods) are able to properly account for the dispersive forces, several of the most famous density functionals (such as B3LYP and BLYP) fails in describing these interactions.[31] Popular tools to account for these effects are the DFT-D, the dispersion-corrected DFT approaches (e.g., Grimme's DFT-D2,[40] DFT-D3,[41,42] and DFT-D4,[43,44] and their variations), which empirically include a term to correct the overall energy.[33] Some examples using DFT-D will be discussed along this review.

Computational chemistry has also helped developing models and descriptors for reactivity that contribute to a deeper understanding of intrinsic molecular features that control reactivity. The activation-strain model (ASM), connected with the energy decomposition analysis (EDA), has become one of the most successful tools to decompose the complex forces acting between reacting species into simpler components, being successfully applied to establish a causal relationship between the structure of reactants and their chemical reactivity. This fragment-based approach decomposes the interaction energy $\Delta E(\zeta)$ between fragments into different terms,

favoring physical interpretation, helping rationalization at a finer level, and contributing to the understanding of the molecular descriptors that control reactivity. In the ASM model, also called distortion/interaction model,[45] the $\Delta E(\zeta)$ is decomposed into two contributing terms along the reaction coordinate (ζ), namely the strain (or distortion), $\Delta E_{strain}(\zeta)$, and interaction, $\Delta E_{int}(\zeta)$, energies. From a practical point of view, the choice of the reaction coordinate might be challenging and the recommendation is to decompose the $\Delta E(\zeta)$ along all the intrinsic reaction coordinate (IRC) projected onto a coordinate that clearly changes along the reaction pathway.[45] The strain (or distortion) is associated with the geometrical deformation needed to take the reactant(s) from its(their) equilibrium geometry to the structure it assumes in the transition state, this being typically a destabilizing factor, which contributes to increase the energy along the reaction coordinate leading from the reactant up to the transition structure. The interaction energy, in turn, may be either attractive or repulsive, usually contributing to destabilize the system at the beginning of the reaction, becoming however strongly attractive as the reaction advances.[46] The interaction energy can be further decomposed into four terms (known as the Energy Decomposition Analysis, EDA):[47] the orbital interaction energy, ΔE_{oi}, the electrostatic interaction, ΔV_{elstat}, the Pauli repulsion energy, ΔE_{Pauli}, and the dispersion energy, ΔE_{disp}, with the latter being usually neglected.[48] The orbital interaction, ΔE_{oi}, accounts for, among others, the orbital interactions between the occupied and virtual orbitals of each fragment, i.e., a charge-transfer interaction. The ΔV_{elstat} is ascribed to the *quasi*-classical electrostatic interaction between the unperturbed charge distributions of the two deformed interacting fragments. Finally, the Pauli repulsion, ΔE_{Pauli}, is often attributed to the repulsive steric interaction between the two deformed fragments. It accounts for the unfavorable interaction between the fully occupied orbitals of each fragment, according to the Pauli Exclusion Principle. Thus, the latter is always a positive (thus destabilizing) component of the interaction energy $\Delta E_{int}(\zeta)$.[49] Readers interested in a deeper description of these approaches are addressed to the following comprehensive reviews.[46,50-53]

Several approaches based on the electron density are also available to analyze the topology of the electrons distribution in a reacting system. For example, the NCI analysis examines non-covalent interactions (NCI) in terms of the electron densities and their reduced gradients.[54-56] Because of the relatively small computational cost associated with this type of analysis, they are particularly useful to be employed for very large systems, such as nanomachines, nucleic acids, proteins and solvated systems.[57] Another popular approach based on the electron density is the Quantum Theory of Atoms in Molecules (QTAIM)[58-60] and Natural Bond Orbital analysis (NBO).[61,62] Both have been used to rationalize unconventional chemical bond connecting reference systems. Modeling the solvent effect on reaction mechanisms is another important feature we would like to highlight, since most reactions occur in solution. Computational chemistry accounts for these effects by two main approaches: implicit and explicit solvation models. While the former simulates the solvent as a bulk continuum (in general, a dielectric),[63,64] the latter explicitly incorporates the solvent molecules around the solute(s) and accounts for their specific interactions. With respect to the required computational costs, implementing the implicit solvation models usually requires shorter simulation times and less advanced hardware.[64,65] However, this oversimplified approach might neglect important specific solute-solvent interactions, such as hydrogen bonds. The usage of hybrid solvation models (that is, mixing the implicit and explicit models) is often an efficient strategy.[66]

Hybrid methods might also provide accurate results for very large systems in a relatively economic way, reason why they became so popular amongst the computational chemists. For instance, processes in solution[66] in which the solvent environment influences the properties of the solute and enzymatic reactions[67] could take advantage from this strategy.[68] The main idea of such methods is to treat various regions of the system at different computational levels assuming that they play different roles in the investigated phenomenon.[69]

In the perspective outlined above, we present a set of examples that show how computational chemistry can be used as a powerful tool to rationalize chemical problems and design processes through reaction mechanisms exploration. We focused on recent works from our own lab and from other researchers. The review is organized according to the following three main subjects: (*i*) support to organic synthesis; (*ii*) support to natural product chemistry; and (*iii*) support to environmental chemistry. For each of these subjects, we offer several examples of experimental-computational interplay, mainly from our own research group, but also from other impactful works that have accented the importance of molecular modeling to understand and predict chemical reactivity.

2. Support to Organic Synthesis

Organic synthesis is an essential area of experimental chemistry dedicated to the preparation of organic compounds. The ongoing progress of this area in the last

century has contributed to profound advances in science and technology, such as the pharmacological and oil industry, material science, and nanotechnology.[1] Its growth is associated with the evolution of spectroscopic techniques (structure characterization) and the understanding of chemical processes at the molecular level. For the rational planning of a new compound or total synthesis of a natural product, it is necessary to have a comprehensive knowledge of the involved reaction mechanisms to allow design efficient synthetic routes. The alliance between experiments and computational simulation can provide a broader and deeper understanding of the structure and properties of organic compounds, as well as the elucidation of the reaction mechanisms.[11,70] Besides those, classical organic reactions have also been reviewed from a computational point of view.[71,72] In the following, we will address how computational chemistry can be used as support for organic synthesis, considering several key points, such as isomerization and thermodynamic stability, reaction mechanism elucidation, selectivity (stereo-, chemo- and regiochemistry), and solvent effect.

A first representative example combining theoretical and experimental data to understand an intriguing observation that we present is the case of *Z*-*E* acid isomerization of γ-alkylidenebutenolides.[73] These are molecules with an α,β-unsaturated γ-lactone moiety substituted by an alkylidene at the gamma position, regarded as an important skeleton to several pharmacological activities.[73] Almost all of their derivatives are reported in the *Z* form, but depending on the synthetic strategy and the solvent used for structure characterization, a *Z*-*E* diastereoisomeric mixture is also observed. Aiming to understand the isomerization process, Varejão *et al.*[73] synthesized seven γ-alkylidenebutenolides, with benzene and substituted furan as aromatic portions. Through experimental high-performance liquid chromatography (HPLC) and ^{1}H NMR analyses, the authors detected an unexpected isomerization process of the most stable (*Z*) to the less stable (*E*) configuration for most systems, after being suspended in organic solvents for 0 to 4 days. They hypothesized that the residual acidity of deuterated chloroform (CDCl$_3$, solvent) could be associated with this behavior.

To rationalize these experimental findings, the thermodynamics of the $Z \rightarrow E$ (the relative Gibbs free energy of isomerization ($\Delta G = G_E - G_Z$)) isomerization was investigated at the ωB97x-D/6-31G(d,p) level, with inclusion of implicit solvation (PCM = chloroform). According to the relative Gibbs free energy of isomerization, the *Z* form is more stable than the *E* form ($\Delta G < 0$). However, in the presence of an acidic media, the protonation of the carbonyl group stabilizes the *E* configuration. In the

protonated form, both the *Z* and *E* isomers are almost isoergonic (ΔG = 0.1-0.7 kcal mol^{-1}), allowing the existence of both forms in equilibrium. Protonation of the carbonyl group also helps reduce the free energy for rotation around the C=C bond (Figure 1a). According to the simulated thermodynamic data, only one system (benzene as aromatic portion) remains in the *Z* configuration, with ΔG ca. -1.8 kcal mol^{-1} in neutral and protonated form. This profile agrees with experimental data, which shows that after standing for a long time, the *Z* form becomes the main product (about 100%).[73]

Esquivel *et al.*[74] also explored the acid effect on the thermodynamic stability of pyrazol-4-ol and isoxazole-4-ol heterocycles. They reported the synthesis of pyrazol-4-ol and isoxazole-4-ol heterocycles, which occurs in 3 steps in acid methanol solution. Although the *N*-phenyl substituted pyrazol-4-ols (R$_1$ = Ph) derivatives were obtained with moderate to high yields (30-85%), no desired product was detected for the carboxamide pyrazol-4-ol systems (R$_1$ = CONH$_2$), which suffer a dehydration reaction to their corresponding pyrazol form. To address this question, the acid dehydration reactions of both pyrazol-4-ol (R$_1$ as phenyl- or carboxamide-) were explored using X3LYP/def2-SVP(C,H)/ma-def2-SVP(N,O) and M06-2X/ma-def2-TZVPP DFT level, with SMD, an implicit charge-density (D) based solvation model (SM) for methanol. They identified that the reaction could pass by four steps (Figure 1b) for both phenyl- and carboxamide-systems. The simulations indicate that the main difference on the energy profile regards the water elimination step (rate determinant step, Figure 1b, step *iii*), in which the computed energy barrier is 3.7 kcal mol^{-1} higher for phenyl- than for carboxamide pyrazol-4-ol. In other words, the dehydration of carboxamide pyrazol-4-ol to their respective pyrazol is 10^2 times faster than the phenyl- one. This energy profile agrees with experimental results about the fast dehydration of carboxamide derivatives.[74]

These illustrative examples show how the reaction media (in these cases, the presence of an acid) has an influence on the thermodynamic (isomerization equilibria) and kinetic (energy barrier) properties of the reaction.[73,74] In the following example, we show how the reactant structure can also control the reaction mechanism type. This is the case of 1,2,3-triazole synthesis from the Sakai reaction.[75] This synthetic protocol is widely employed in 1,2,3-triazolone synthesis from α,α-dichlorotosylhydrazones and amines. Despite of being extensively used, the reaction mechanism is still unclear. The main mechanistic proposal starts from a chloride elimination to form a vinyldiazine as key intermediate. Then, the reaction can follow two paths to the amine addition, as proposed by Sakai[76] and Hanselmann[77] (Figure 1c).[76,77] On
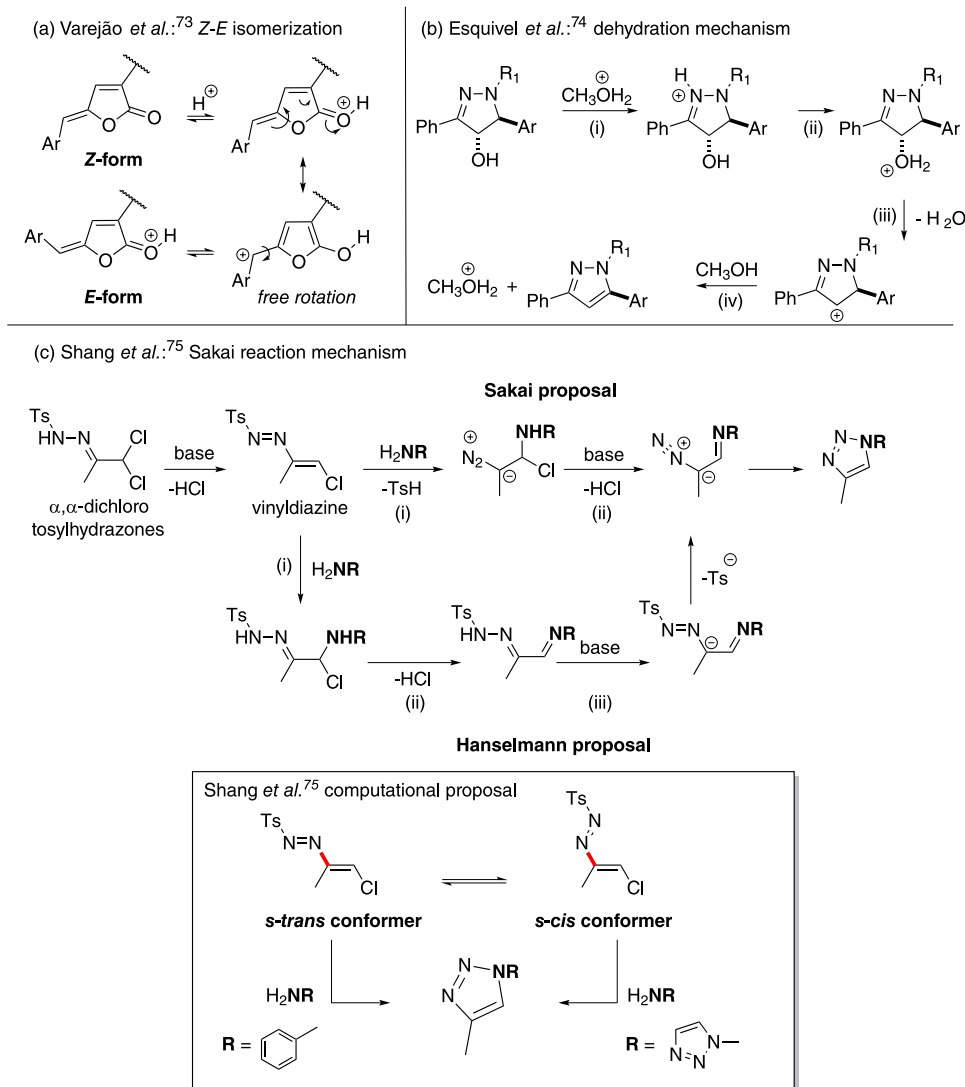
Figure 1. (a) *Z-E* isomerization of γ-alkylidenebutenolides in acid media; (b) mechanism for the dehydration of pyrazol-4-ol; (c) relevant intermediates for the Sakai reaction mechanism proposed by Sakai,[76] Hanselmann[77] and Shang[75] (C–N bond highlighted in bold red).

the Sakai pathway (Figure 1c), the -tosyl liberation occurs concerted with the amine attack (step *i*), followed by the base-induced elimination of chloride (step *ii*). In contrast, in the Hanselmann mechanism (Figure 1c), the -tosyl group leaves only after the amine attack (step *i*) and chloride elimination (step *ii*). The neutral intermediate formed in step *ii* was detected by X-ray diffraction, supporting the Hanselmann mechanism. Nevertheless, computational evaluations showed that the direct amine attack cannot occur before chloride elimination and the whole process depends both on the *cis/trans* configuration of the vinyldiazine intermediate and the amine structure.

In addition to the uncertainties concerning the reaction path, the amine has a great influence on the reaction yield. Thus, Shang *et al.*[75] explored computationally the Sakai reaction with two different amines (H₂NR, R = benzene and triazol) using B3LYP-D3/6-311+g(2d,p)//

B3LYP-D3/6-31G(d) computational method with the simulation of the implicit solvent medium (methanol, SMD model). They identified that both Sakai and Hanselmann proposals has energetic inconsistences, as the liberation of the -tosyl group (Sakai path) and the direct attack of the amine (triazolamine) in the first step (Hanselmann path) are difficult to occur. For -tosyl liberation, there was a consistent energy increase with the elongation of the N–S bond (higher than 20 kcal mol⁻¹). For the pathway involving the amine attack, the authors did not identify the formation of a stable intermediary in step *i*, as proposed by Hanselmann. Shang calculations[75] showed that a key point in the reaction mechanism is the rotation of the C–N bond (highlighted in bold red) in the vinyldiazine intermediate (Figure 1c, Shang computational proposal) with the amine working as a nucleophile. When the amine is triazolamine, only the *s-cis* conformer of vinyldiazine allows the direct

attack, similar to the Hanselmann pathway, but with a high energy barrier (about 23 kcal mol^{-1}). For the aniline, the direct attack in both *trans* and *cis* conformation is feasible (15-20 kcal mol^{-1}), occurring with a lower energy barrier, due to charge stabilization. The pathway starting from the *trans* form and with aniline as a nucleophile has the lowest energy barrier, being the ideal condition for the synthetical protocol. The theoretical calculations using different amines were able to predict which one is most favorable (following the *trans* path) to form triazole rings in the Sakai reaction.[75]

Organocatalysis is a major topic within organic synthesis, once organocatalysts are substances that are easily accessible, simpler, and usually less toxic than either enzymes or metal catalysts.[78,79] A promising type of organocatalysts that has shown efficiency in organic synthesis are the *N*-heterocyclic carbenes (NHCs), which are being used with different goals.[80-82] As an example, NHCs are being employed in polymer synthesis, such as in the synthesis of poly(δ-valerolactone), produced from the polymerization of δ-valerolactone.[83] Recently, the polymerization of δ-valerolactone was investigated in our group exploring the NHC role in the absence and the presence of a co-initiator (alcohol) by means of DFT at the N12SX/6-311+G(d,p) level, simulating water as solvent with the implicit solvation Integral Equation Formalism variant of the Polarizable Continuum Model (IEFPCM) method.[84] The hypotheses were that the NHC could either act as nucleophile, directly opening the lactone ring, or as a Brønsted base, activating the barely acidic hydroxyl group of the alcohol. In the direct attack of the NHC on the lactone, the NHC acts as a nucleophile and attacks the lactone to form a zwitterionic intermediate, as depicted in Figure 2a. The simulations suggest that the rate determining step (rds) for the first route (direct attack) is the ring opening, however with a high energy barrier (18.4 to 37.4 kcal mol^{-1}), being also highly endothermic. For the alternative route (activation of the co-initiator), the features of the NHC, in particular their basicity, play a pivotal role to the rds. For most NHCs, with intermediate basicity, the rds is the first step, characterized by a termolecular transition state, involving the nucleophilic attack of the alcohol activated by the NHC. For NHC with high basicity, as determined by proton affinity simulations, the lactone ring opening (second step in this route) is the rds, as the nucleophile activation (i.e., proton abstraction) is favored. Even so, energy barriers are smaller than for the direct route (from 2.2 to 15.0 kcal mol^{-1}), agreeing with experimental evidence that showed faster ring-opening polymerization with alcohol as a co-initiator.[84,85]

The organocatalytic field has gained great visibility in recent years due to the contributions mainly of List and MacMillan.[78-87] Their work with organocatalysis in asymmetric synthesis revolutionized this field, awarding them the Nobel Prize in 2021 for the development of asymmetric organocatalysis.[88,89] The popularization of this theme made it one of the main branches of enantioselective synthesis, being a powerful alternative for enzymatic and organometallic catalysis. As just stated, NHCs constitute an important class of organocatalysts. He *et al.*[90] explored the chiral structures to the asymmetric β-carbon functionalization of carboxylic esters through [3 + 3] cycloaddition to form δ-lactams in high yields (97%) and high enantioselective character (98% of enantiomeric excess, *ee*) (Figure 2b). To address the origins of the enantioselectivity, Li *et al.*[91] carried out molecular simulations at the M06-2X-D3/6-311++G(2df,2pd) level, using tetrahydrofuran (THF) as an implicit solvent (IEFPCM). According to their results, the most reasonable mechanism comprises seven steps, in which the first one is the NHC binding to the ester and thus making it more electrophilic, while the last step is the catalyst regeneration (NHC liberation), Figure 2b. They concluded that enantioselectivity arises in the carbon-carbon bond formation step, controlled by noncovalent C−H···O, C−H···N, and π-π interactions. The stereo controlling step to form the *S* product (*Si* face attack) has the lowest energy barrier (14.6 kcal mol^{-1}) compared to any other assessed possibility. By the simulated energy barriers, the authors estimated 98% of enantiomeric excess (*ee*), the same value reported experimentally. These results are useful to design new reactions and chiral NHC organocatalysts.[91]

One of the most powerful class of reactions to build new molecules are the cycloadditions, due to their synthetic versatility, regio- and stereochemical control and ability to provide formations of multiple bonds. Besides the classical [4 + 2] cycloaddition to form a six-membered ring, largely explored by Diels and Alder, the construction of systems with other sizes, such as [4 + 3], is also paramount.[92,93] Depending on the experimental conditions, different types of cycloaddition reactions may compete. This is the case of the [4 + 3] and [3 + 2] intramolecular cycloaddition of epoxy and aziridinyl enolsilanes. In standard conditions to [4 + 3] cycloaddition, the [3 + 2] cycloadduct was formed exclusively and with high diastereoselectivity (92% *ee*).[94] Chen *et al.*[93] explored a variety of epoxy and aziridinyl enolsilanes under cycloaddition conditions. They found high chemoselectivity for the *trans*-fused [3 + 2] cycloadduct, while no [4 + 3] cycloaddition was identified. DFT calculations of the reaction mechanism at M06-2X/def2-TZVPP/SMD(DCM)//B3LYP-D3(BJ)/6-31G(d,p)/CPCM(DCM) level was employed to elucidate the diastereo- and chemoselectivity. According to their results,
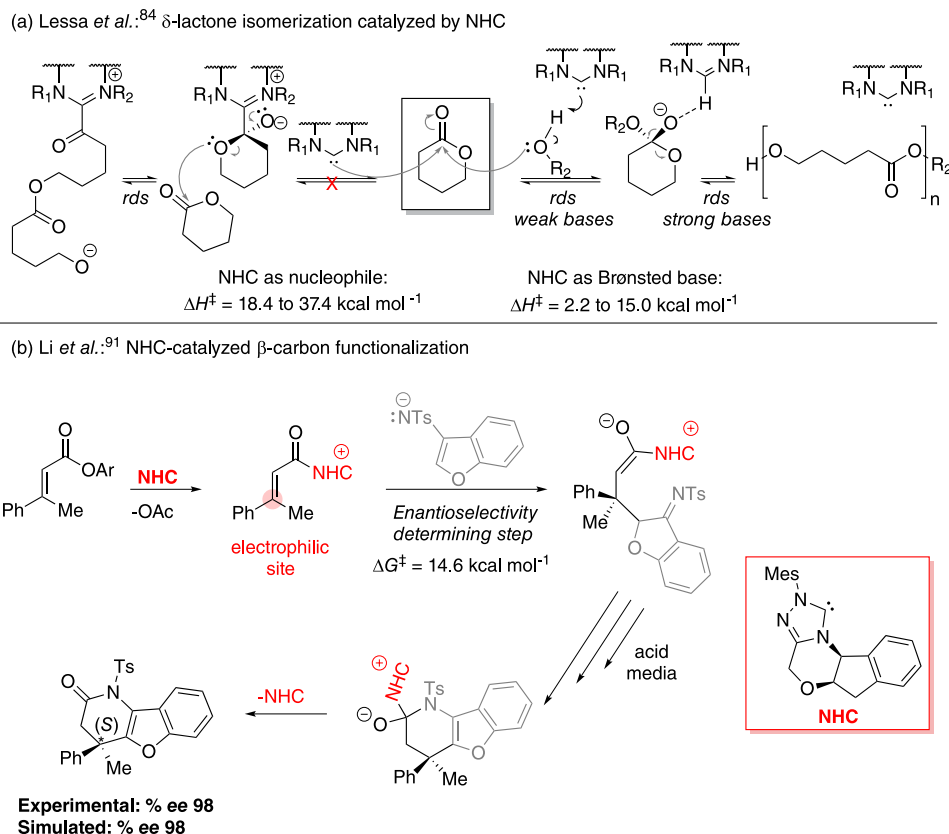
Figure 2. (a) Two possible mechanisms for ring-opening polymerization of δ-valerolactone assisted by NHC; (b) [3 + 3] cycloaddition reaction catalyzed by NHC.

the diastereoselectivity is associated with the C–C bond-forming step (Figure 3a, step *i*), which has activation energy to form the *exo* intermediate lower than the corresponding one to form the *endo* intermediate (ΔΔG‡ = 1.2 kcal mol^{-1}). The *endo* transition state (TS) is destabilized by torsional strain related to 1,3-diaxial interactions, while the *exo* TS is almost staggered. The chemoselectivity can also be rationalized in terms of kinetic factors: formation of [3 + 2] cycloaddition requires 4 kcal mol^{-1} less energy than formation of the [4 + 3] intermediate (Figure 3a, step *ii*). The TS leading to the *endo* intermediate is geometrically different from the one leading to the *exo* key intermediate, then the major structural reorganization in this path is unfavorable to the [4 + 3] product. These theoretical findings allowed the authors to design new systems that favored the [4 + 3] products.[93] Cycloaddition competitions can be associated with different structural factors. Alnajjar and Jasinski[95] fully explored [2 + 1] and [4 + 1] cycloaddition competition in the reaction between nitroalkenes and dichlorocarbene by DFT at the B3LYP/6-31G(d) level. Their evaluations show that the competition is possible only for reactions with 2-substituted nitroethene systems. For nitroethene itself and its 1-substituted analogs, [2 + 1] cycloaddition is the only possible scheme, as

[4 + 1] is kinetically less favorable, as indicated by the activation Gibbs free energy of ΔG‡ = 12.8 for [2 + 1] and 18.3 kcal mol^{-1} for [4 + 1] cycloaddition. Further, the [2 + 1] cycloaddition has a non-polar character (biradical TS), while the [4 + 1] one has polar transition structure (zwitterionic TS).[95] This radical character in cycloaddition reactions was also reported by Fiorot *et al.*[96]

The previous examples show how computational chemistry can give insights into organocatalytic processes. Besides the catalyst activity, the product structure provides insights to decipher the reaction mechanism. For instance, one can use the absolute configuration of a given product to differentiate an aliphatic nucleophilic substitution mechanism between the uni- (S$_N$1) and bimolecular (S$_N$2) pathways.[97,98] In the S$_N$1 mechanism, the formation of a carbocationic planar intermediate allows the nucleophile approaches by both sides, yielding a racemic mixture. On the other hand, the S$_N$2 pathway usually is an asynchronous concerted process and generally leads to a product with inversion of configuration (backside approach preferred).[99] Although these mechanistic features are well established, in some cases observations might be tricky to rationalize, as in the following example. Evangelista *et al.*[100] conducted several synthetic and computational experiments to

evaluate the reaction mechanism of azide (N_3^-) insertion into a benzodiazepine derivate. They employed different reaction conditions (leaving group, solvent, temperature, and reaction time) to modulate product formation. They showed that temperature has a major influence on the stereochemical features of the reaction pathway (Figure 3b). When they performed the experiments at 55 °C, the reaction yields a product with 100% configuration inversion, regardless of the employed reaction condition. At 100 °C, they obtained product with a ratio of 36:64 in terms of retention:inversion. By increasing the reaction temperature to 120 °C, the major product is the one with retention of configuration (63:37 ratio). To rationalize these unprecedent observations, they employed molecular simulations at the M06-2X/6-311+G(d,p) level. The S_N1 pathway was immediately disregarded, as the carbocation formation is endothermic by a large amount (almost 45 kcal mol^{-1}). Conversely, the computed energy barrier in terms of enthalpy for the S_N2 pathway (displacement of the OMs (methanesulfonate or mesylate) by the N_3^- nucleophile) is lower (19 kcal mol^{-1}) than for the S_N1 pathway, forming the product with a first configuration inversion. On higher temperatures, a second S_N2 substitution reaction may occur, restoring the initial configuration. Computation revealed that the azide nucleophile may displace the azide-substituted product with an activation energy of 31 kcal mol^{-1}.[100]

Batalha *et al.*[101] studied the regioselectivity of the *N*-ethylation reaction of *N*-benzyl-4-oxo-dihydroquinoline-3-carboxamide, a useful reaction to produce *N*-alkyl substituted compounds. In this case, although two nitrogen atoms are available to react as nucleophiles (N^1 and $N^{3'}$, in Figure 3c), the reaction exclusively produced only the product with *N*-ethylated at the $N^{3'}$ position (80%). The regioselectivity was assessed by DFT calculations (B3LYP/6-31+G(d)/IEFPCM = dimethyl sulfoxide (DMSO)) of the acidity of the N^1–H and $N^{3'}$–H unities and the activation energy for the possible ethylation at both reaction sites. Analysis of the preferential deprotonation sites indicates that the regioselectivity is associated with the higher N^1–H acidity of oxoquinoline portion as compared to the $N^{3'}$–H of the carboxamide moiety. The computations indicate that deprotonating the N^1–H unit is preferred by more than 22 kcal mol^{-1} as compared to deprotonation of the $N^{3'}$–H (Figure 3c). Because of the lower stability (that is, higher energy) of the carboxamide conjugated base, the *N*-ethylation from this site occurs with a lower activation barrier (more reactive). The computed activation energies are 9.5 kcal mol^{-1} for the $N^{3'}$-ethylation and 11.4 kcal mol^{-1} for the N^1-ethylation.[101]

Yet regarding regioselective aspects of an organic transformation, Delarmelina *et al.*[102] combined experimental and computational investigations to rationalize the preferential formation of the α-lapachones over the β-isomer in the hetero-Diels-Alder (HDA) reaction between an *o*-quinone methide and a set of dienophiles (Figure 3d). After exploring the reaction between the *o*-quinone methide and the dienophiles, the authors observed a consistent selectivity towards the α isomer (77-80%), despite of the chemical similarity of the two possible reactant sites. The theoretical calculations indicated that the origin of selectivity has a kinetic reason, that is, the formation of the α product has a lower activation energy than the barrier for formation of the β analogue.[102] The activation strain model (ASM) and the energy decomposition analysis (EDA) were applied to rationalize these results. While the ASM revealed that diene-dienophile interactions control the regioselectivity, the EDA results points that the barrier height is associated mainly with Pauli (steric) repulsion: the α-TS has a less destabilizing Pauli repulsion than the β-TS. Furthermore, the authors also explored the *endo/exo* diastereoselectivity and *ortho/meta* regioselectivity of the hetero Diels-Alder reaction in 3-methylene-1,2,4-naphthotriones. For all cases, diastereoselectivity was discrete, with a small energy difference between the *endo/exo* energy barriers ($\Delta\Delta G^{\ddagger} < 4$ kcal mol^{-1}, *endo* favorable). On the other hand, *ortho* regioselectivity was considerably favored for all systems, with a pronounced effect of the substituent electron donating groups (EDG) ($\Delta\Delta G^{\ddagger}$ about 19 kcal mol^{-1}). This was associated with the dienophile approximation over the diene: *ortho* approximation induces a dipole moment that can be stabilized by EDG of the dienophile.[102] This deeper exploration of the energy profile through ASM and EDA has been widely used in the literature to understand the mechanisms of organic reactions.[51,52,72,103]

All the studies mentioned above explore reactions in an implicit medium. That is, only one bulk property of the solvent is simulated (e.g., dielectric constant). This allows simulating the average effect of the solvent field and its influence on electronic and structural properties of the solute, such as attenuation of atomic charges and small structural changes as a function of the medium.[65,104,105] Despite being the most used solvation model in computational chemistry, this model fails to describe important solute-solvent interactions. An alternative is to use explicit solvation, in which solvent molecules are explicitly considered throughout the simulation. Regarding to reaction mechanism simulations, the implicit-explicit solvation approach (known as microsolvation) is a good alternative to simulate both bulk properties and relevant solvent-solute interactions by including only a few explicit solvent molecules associated with implicit solvation models (IEFPCM, SMD, Conductor-like Screening Model (COSMO), etc.).[65]
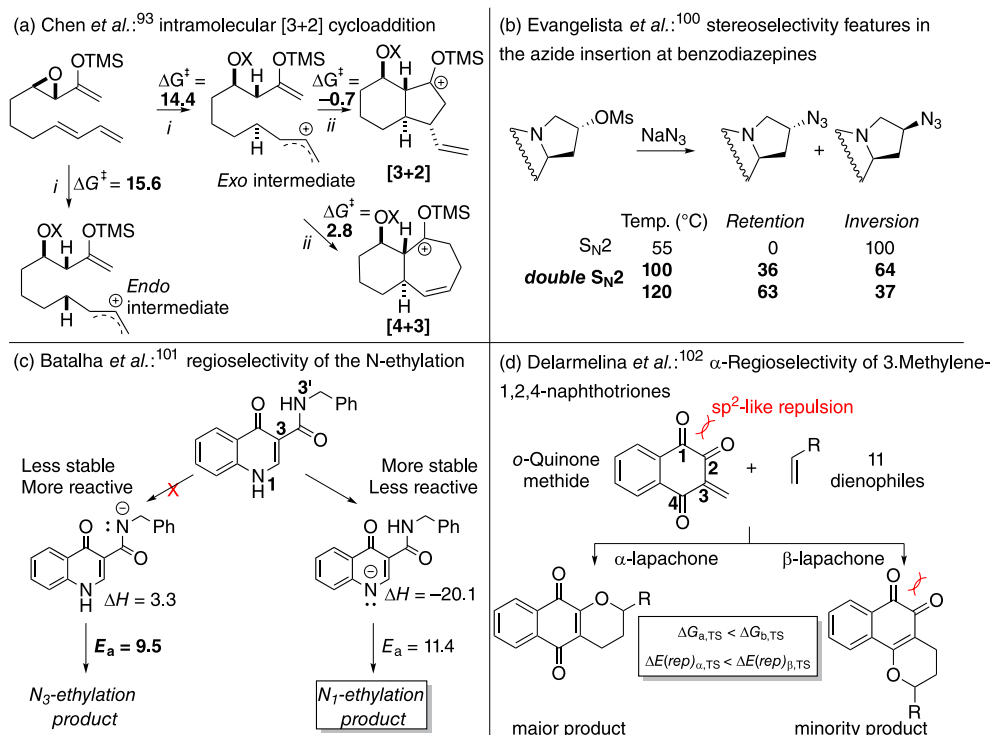
Figure 3. (a) Competition between intramolecular [3 + 2] and [4 + 3] cycloaddition pathways of epoxy and aziridinyl enolsilanes; (b) temperature effect on diastereoselectivity of nucleophilic substitution; (c) conjugated bases of N_3- and N_1-ethylation reaction of oxo-dihydroquinoline-carboxamide; (d) α-regioselectivity of hetero-Diels-Alder reactions. Energy values reported in kcal mol^{-1}.

The α- and β- lapachone isomerization was previously discussed regarding their HDA reaction. In that case, the authors specifically explored the formation of the product as a function of different dienophiles.[106] However, the reaction medium has a great influence on isomerization, which was also explored by Delarmelina *et al.*[103] They combined experimental and DFT approaches to understand the switchable regioselectivity of the acid-catalyzed lapachol cyclization and its α-/β- isomerization (Figure 4a).[106] Experimentally, when dilute solutions (HCl/AcOH 9 and 18%, H_2SO_4 25 and 50%) are used at room temperature (r.t.), a mixture of α- and β- isomer was identified, with α- percentage increasing over time. On the other hand, for higher acid concentration ($H_2SO_4 > 75\%$), the majority product was the β-isomer (86-100%). Theoretical calculations were made at B3LYP/6-31++G(d,p) level to understand the origin of the isomerization at the molecular level. As the acidic media has huge influence on switchable regioselectivity, the authors employed the microsolvation approach (implicit-explicit solvation). They added explicit molecules considering the possible ion pairs in acidic solution, such as $H_3O^+ \cdots (H_2O)_n \cdots B^-$ ($B^- = Cl^-$, HSO_4^- or SO_4^{2-}). The cyclization process occurs with low energy barrier (lower than 8.0 kcal mol^{-1}), passing by a deprotonated key intermediate. The α/β isomerization was calculated for both dilute and concentrated acid medium,

with H_2O and HSO_4^- as bases, respectively (Figure 4a). In dilute medium (2 explicit water molecules), the energy profile relative to the key intermediate is very similar, with calculated enthalpies barriers of α → β of 15.1, and β → α equal to 14.2 kcal mol^{-1}. Nevertheless, the α isomer is slightly more stable than the β isomer (enthalpy change of $\Delta H = -0.9$ kcal mol^{-1}) and is formed with smaller activation energy. This agreed with experimental identification of the α/β isomer mixture and slow conversion of the β- into α- isomer over time. Calculations with explicit HSO_4^- (concentrated media, 2 explicit HSO_4^- ion), showed enthalpy activation of $\Delta H^\ddagger = 11.5$ and 11.7 kcal mol^{-1} for α → β and β → α isomerization, respectively. Under these conditions, the β-isomer is 0.2 kcal mol^{-1} more stable than the α isomer. So, in concentrated acid, the β-isomer is the major product due to small activation energy and higher thermodynamic stability. Although these energy differences are small, the calculated energy profile for both conditions agree with the experimental data.[106]

Solute-solvent interactions can modulate the products depending on the interaction site, as we pointed out in the previous example. Furthermore, the explicit consideration of solvent can give insights about alternative pathways leading to the same product. Fiorot *et al.*[107] explored this case in the synthesis of 1,3-dioxanes, which are an important class of heterocycles. These compounds are usually

synthesized by the Prins cyclization reaction, in a classical reaction mechanism which are reported as passing through carbocationic structures. However, previous computational studies pointed out that those ionic intermediates might not be found on the minimum energy path, and that hemiacetal intermediates are more stable under acid catalysis.[108] Thus, Fiorot explored a Prins-like reaction to 1,3-dioxanes synthesis in aqueous media, with benzenamine and acetaldehyde (1:3) as starting material. The target reaction is environmentally friendly (no catalyst) and was reported with high yields (85%). They employed the DFT ωB97X-D/6-311++G(d,p) method with microsolvation approach (implicit + explicit solvation) to simulate water as solvent. Metropolis Monte Carlo calculations were carried out aiming to assess the first solvation shell (3-5 explicit water molecules) in key intermediates with charged species and prototropism processes. According to their evaluations, the first step is the enamine formation, which is less stable than the initial complex ($\Delta H = 8.8$ kcal mol^{-1}) and is formed with low activation energy (rds $\Delta H^{\ddagger} = 8.8$ kcal mol^{-1}) (Figure 4b, step *i*). Next, the nucleophilic attack on a second acetaldehyde (rds $\Delta H^{\ddagger} = 12.2$ kcal mol^{-1}) can form two final products, in neutral and zwitterion forms (Figure 4b, step *ii*). The equilibrium is shifted to the neutral form, which is more stable by 13.5 kcal mol^{-1}. Despite that, the authors explored the complete reaction mechanism starting from both structures. According to their evaluations, the ionic pathway is kinetically and thermodynamically unfavorable, while the non-ionic path has small energy barriers and passes by a hemiacetal intermediate (as reported previously for catalyzed cyclization.[108] Such a path is made possible by the interactions with the explicit solvent, which enables prototropism processes throughout the reaction. The same reaction profile was identified for others amines, such as *p*-nitroaniline, *p*-methoxyaniline and methylamine. The authors also provided theoretical kinetic isotope effect (KIE) to be used as a reference data for further experiments.[107]

In cases of competitive mechanisms, the number of simulated solvent molecules may favor one mechanism over the other, specifically in competitive paths, such as bimolecular nucleophilic substitution (S$_N$2) and base-induced bimolecular elimination (E2). The S$_N$2 *versus* E2 competition was computationally explored by Hansen *et al.*[103] They selected a representative reaction, with fluoride (F$^-$) as nucleophile and ethyl chloride (CH$_3$CH$_2$Cl) as substrate, aiming to identify the influence of progressive explicit solvation (S$_n$, n = 0-3 explicit solvent molecules). To do so, the DFT ZORA-OLYP/QZ4P level was employed and the implicit solvation (bulk solvent effect) was simulated with the COSMO model. Nonpolar
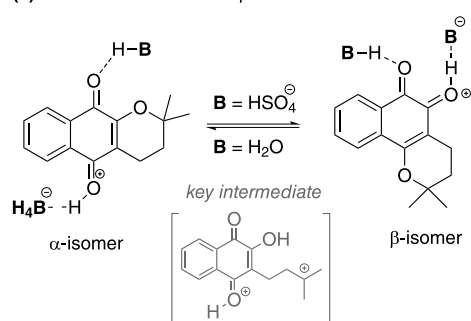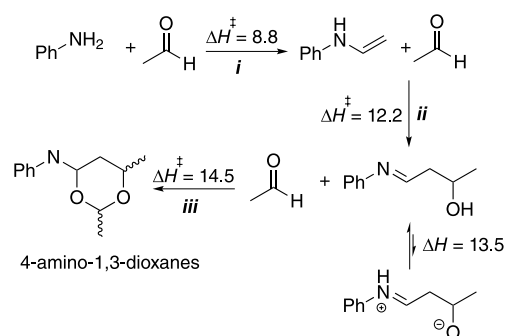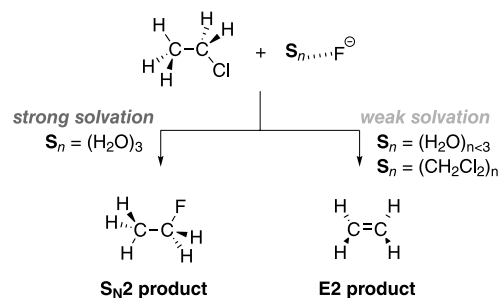
Figure 4. (a) Media influence on α/β isomerization of lapachones; (b) key intermediates for Prins cyclization and 1,3-dioxanes synthesis; (c) S$_N$2/E$_2$ products depending on the solvent media. Energy values reported in kcal mol^{-1}.

aprotic (CH$_2$Cl$_2$) and polar protic (H$_2$O) solvents were select to represent realistic solvation extremes. According to their results, the increase in the number (n) of the explicit solvent molecules promotes the increase of the energy barrier. This is due to the reduction in intrinsic nucleophilicity and protophilicity of the fluoride ion under solvation. The E2 mechanism was calculated as the preferred path in most cases (weaker solvation), with $\Delta\Delta G^{\ddagger} = -7.1$ to -2.0 kcal mol^{-1} (compared to S$_N$2). Only for strong solvation, i.e., (H$_2$O)$_3$, the S$_N$2 is favored, with a small energy barrier compared to E2, with $\Delta\Delta G^{\ddagger} = -2.2$ and -3.8 kcal mol^{-1}, with and without implicit solvation, respectively (Figure 4c). To fully elucidate the solvation effect, they employed the activation strain model and energy decomposition analysis. They identified that the E2

pathway has a higher distortive character than S_N2, once in this pathway, two bonds are broken in the substrate. On the other hand, solvation has an effect on fluoride stabilization, reducing its basicity. Thus, when we use strong solvation, the basicity is highly reduced and the substrate-nucleophile interaction is compromised. As the E2 mechanism is already disadvantaged by distortion, the reduction of basicity in strong solvation becomes an extra destabilizing factor, causing the energy barrier to increase compared to S_N2 in that media.[103] This S_N2/E2 competition was also explored by Lisboa and Pliego[109] for complex microsolvated environments, such as *tert*-butanol explicit molecules.

3. Support to the Chemistry of Natural Products and Biochemical Transformations

Natural products are secondary metabolites structurally diverse substances displaying unique properties, inspiring academic and industrial synthetic chemists to produce compounds with a wide range of applications over the years.[10,110] Following this standpoint, the growing possibility of substrates, catalysts, and reaction pathways associated with the demand for more efficient and environmentally friendly methods reached a point where it is impractical to carry out researches limited to experimental approaches.[111-113] In this section, we highlight some of the chemistry of natural products computationally aided in which the assessment of reaction mechanisms helped to solve experimental issues.

The structure elucidation is one of the biggest issues to natural product chemistry. Although the advent of modern spectroscopic techniques made this task easier, for some complex frameworks where different stereoisomers are possible, the structure determination remains challenging. In this sense, several works report the structure reassignment of natural products.[114,115] The simulation of spectroscopic properties and reaction pathways has revolutionized the area.[116] In 2020, our research group[117] carried out computational simulations to investigate Pettus and co-workers[118] hypothesis that the helianane family, a class of natural products with anticancer activity, would have its structure originally misassigned in 1997 by Harrison and Crews.[119] These substances are extracted from the marine sponge *Haliclona fascigera*. In this study, employing molecular modeling techniques is a particularly useful strategy since these compounds are rare and difficult to obtain. The calculation outcomes corroborated with Pettu and co-workers[118] hypothesis. Their ^{13}C NMR theoretical analyses pointed out a similarity between the spectrum of the isolated compound and

synthetic curcudiol, another natural product. Hence, they simulated the most plausible biosynthetic route starting from curcuphenol, trying to reach curcudiol and helianane. For the mechanism investigation, they employed the DFT level with the ωB97X-D functional combined with the 6-31++G(d,p) basis set. To simulate the aqueous media, the effects of water in the stabilization of the ionic intermediates were accounted for by explicit microsovation with three water molecules. The computations showed that curcudiol is thermodynamically preferable over helianane, being 8 kcal mol^{-1} more stable (Figure 5a).[117] Thus, although it is not possible to fully confirm the hypothesis without reisolating the compounds, the computational work strongly supported it.

Czajkowska-Szczykowska and co-workers[120] studied alkaloids with several potential pharmacological activities from the genus as *Solanum*, used as diuretic, antispermatogenic, antiandrogenic and antifungal. Interestingly, some *Solanum* steroidal alkaloids, e.g., solasodine, have a spiro unity, usually challenging to synthesize in a laboratory. They revised the structure of the *N,O*-diacetylated solasodine derivative after detecting an unusual epimerization ($22R \rightarrow 22S$) at the spiro atom (Figure 5b) by X-ray diffraction analysis. The authors explored possible reaction pathways related to the inversion of configuration at the spiro carbon (acetylation and deacetylation of solasodine) at the ωB97X-D/6-31G(d,p) level. According to their results, the rds for the epimerization is the C−C bond rotation (Figure 5b, step *iii*), which needs ca. 16 kcal mol^{-1}. The ring-closing step *iv* occurs almost barrierless, leading to the 22*S* product. In basic medium, the inverse reaction is favored (return to 22*R* form) since there can be deacetylation from the absorption of the acetyl moiety by a strong base (e.g., BuO$^-$). The deacetylation path has a similar intermediates and energy profile, with a C−C rotation energy barrier also around 16 kcal mol^{-1}. As the barrier heights of the inverse and direct paths are similar, the species establish an equilibrium in a basic medium.[120]

Lei *et al.*[121] investigated dyotropic rearrangement of β-lactones to form α-methylene-γ-butyrolactones (MBL), that represent a family of over 5000 natural products. They evaluated the reaction for 75 α-methylene-β-lactones in a previously optimized reaction condition (Lewis acid: EtAlCl$_2$, solvent: Et$_2$O). According to their experimental results, the substrate structure strongly influences the rearranged product. For R$_1$ = H, a migration of hydrogen occurs, forming the BML (5,5-dialkyl-substituted) product with high yields (60-86%). However, R$_1$ = aryl forms the 4,5-diaryl substituted MBL with most yields around 90%. Figure 5c shows the two products as a function of the substituents. They explored the reaction mechanism employing DFT, using the PWPB95-D3/def2-QZVPP//

PBE0-D3/def-TZVP method and SMD implicit solvation model in Et$_2$O media. Their simulations showed that hydrogen migrates concertedly with the ring expansion to form the BML with activation free energy of about 23 kcal mol^{-1}. On the other hand, the aryl-migration favors the stepwise pathway passing through a stabilized phenonium ion intermediate to form the MBL products: the ring opening (denoted by the step *i* in the TS of Figure 5c) precedes the R$_1$ migration (Figure 5c, TS, step *ii*). The stepwise pathway is feasible for these cases because of the ability of the substituent to stabilize the ionic intermediate and active participation of Lewis acid EtAlCl$_2$.[121]

Natural products could also be used as a source of greener catalysts to assist the synthesis of organic compounds. Terra *et al.*[122] employed natural organic acids (NOAs) as catalysts in the green synthesis of xanthenones through a one-pot tricomponent protocol under solvent-free conditions from aldehydes, cyclic 1,3-dicarbonyl and phenolic compounds. The xanthenones comprise a class of oxygenated heterocycles present in several bioactive compounds (antiviral, anti-microbial, and anti-proliferative activities, to cite some),[123-126] usually synthesized by non-environmental-friendly methods (see the work of Terra *et al.*[122] for an extensive list of examples). Aiming to develop a green protocol to produce this important moiety, the authors resorted to the NOAs, biodegradable metabolites found in many organisms.[127,128] Terra *et al.*[122] performed an unprecedented computational assessment of the probable mechanism that convert their reagents (dimedone, β-naphthol, and benzaldehyde derivatives) into xanthenones to rationalize the role of the NOAs as catalysts and regioselectivity aspects of this reaction (Figure 5d). By HF/6-31G(d) and LC-ωPBE/6-311++G(d,p) calculations, the authors proposed that the regioselectivity is thermodynamically- and kinetically-controlled in the nucleophilic addition of the carbon 2 (not the carbon 10) of β-naphthol to the carbonyl of the benzaldehydes protonated by the NOAs. The simulated reaction pathway to the C2•••C=O bond formation (pathway *a*) has a lower free energy barrier ($\Delta\Delta G^{\ddagger} = 8.7$ kcal mol^{-1}) and yields a more stable precursor (Int) that precedes the formation of the final xanthenone ($\Delta\Delta G = 10.1$ kcal mol^{-1}) than the simulated for the regio-divergent pathway *b* (C10•••C=O).[122]

The asymmetric total synthesis of natural products has always been a hard task. Computational chemistry can provide information regarding the energetic and structural features of biosynthetic transformations that might be useful in the synthetic lab. In this context, Nakajima *et al.*[129] employed DFT calculations to simulate biosynthesis of several resveratrol dimers, natural products extracted from grapes with chiral complex structures and several pharmacological activities (anticancer, antioxidant, agents against cardiopathies). By using the ωB97X-D/6-31 G(d,p) method, with water as solvent (SMD), chosen after a benchmark evaluation performed with other functionals and using *ab initio* calculations as a reference, the authors identified inconsistencies in the current mechanistic proposal for the formation of the key intermediates vaticahainol A and B. This, in turn, foreseen amendments in their chemical structures. As outcome, the authors established synthetic route to achieve key intermediates to the formation of resveratrol dimers, in addition of supplying new insights into the biosynthetic pathways.[129]

Carotenoids are important components of the cosmetic, nutritional, and pharmaceutical industries.[130] Carotenoids derivatives, such as astaxanthin, can be extracted from microalgae. The commercial synthetic product is a mixture of enantiomers and *meso* compounds. However, the mixture is not approved for medical purposes, only pure (3*R*,3'*S*)-astaxanthin can be used as an antioxidant, anti-inflammatory, antitumor, antihypertensive and antidiabetic. An efficient synthetic methodology to obtain pure astaxanthin (76% yield) has been reported, which pass through the intermediate *meso*-zeaxanthin (95% yield). To understand the isomerization and oxidation process and their stereochemical aspects (Figure 6a), simulations at the M06-L/6-311+G(2d)//M06-L/6-31G(d) level were conducted, including the PCM implicit solvation model with *n*-butanol as solvent. The DFT simulations computed an activation enthalpy around 18 kcal mol^{-1} for the base-induced isomerization process between the (3*R*,3'*R*,6'*R*)-lutein and the (3*R*,3'*S*)-zeaxanthin, which would proceed via a deprotonation at C-6' followed by a protonation at C-4'. This low activation energy suggests that the proposed mechanism for the isomerization is reasonable. For the final oxidation conversion of zeaxanthin into (3*R*,3'*S*)-astaxanthin, the authors observed that upon UV irradiation (365 nm) the yield increased by 8%, which suggested a free radical mechanism for the oxidation. To assess the thermodynamic viability of this mechanistic proposal, the authors performed open shell calculations considering the involvement of free radicals, such as OH• and I•, along the reaction course. The outcomes point that all steps are exergonic by more than 3 kcal mol^{-1}, indicating that the radical mechanism is feasible.[130]

Previously used in Chinese folk medicine with antiproliferative and anti-inflammatory potentials, *Physalis minima* L. is source of compounds such as physalins (C$_{28}$-steroids) with wide range of pharmacological properties, used for treating colds, fever, sore throats and asthma.[131] Wu *et al.*[131] explored the tautomerization mechanism of physalin compounds through DFT
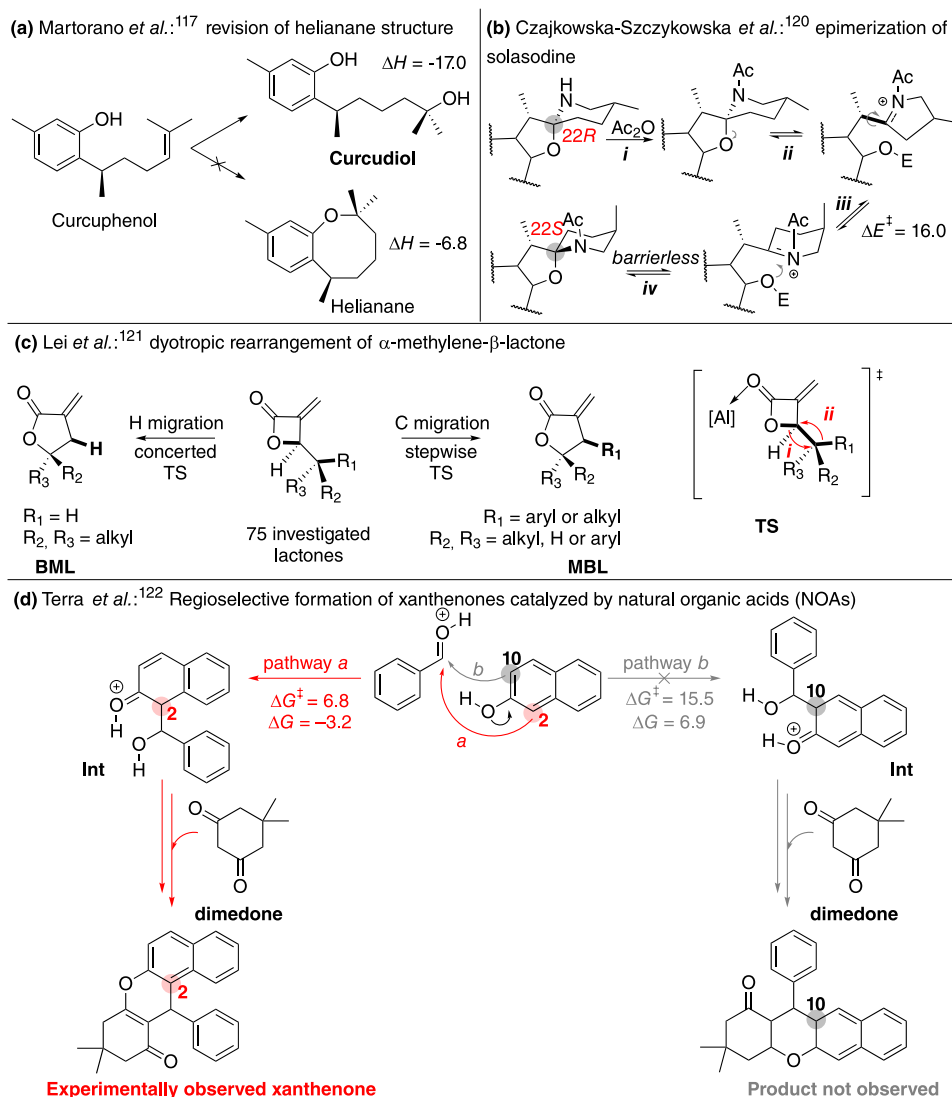
Figure 5. (a) Revision of helianane structure against the biosynthetic pathway; (b) epimerization of solasodine during the acetylation; (c) dyotropic rearrangement of α-methylene-β-lactones to form MBL. Reported energies (ΔG/ΔH); (d) regioselective formation of xanthenones catalyzed by natural organic acids (NOAs). Energy values reported in kcal mol⁻¹.

calculations and isotopic labeling experiments. They employed the M06-2X/6-31+G(d,p) method and implicit/explicit microsolvation (SMD model/one water molecule). The tautomerization occurs via an oxa-Michael addition-proton transfer cascade, in which the rate-determining step (rds) is an intramolecular addition step with activation free energy of 26.6 kcal mol⁻¹ (Figure 6b). As these reactions occurs in water medium, the proper simulation of the solvent molecules, i.e., explicit microsolvation approach, is fundamental to the correct description of the process.[131]

Zhang *et al.*[132] studied the biotransformation of macrolactones through cycloaddition reaction catalyzed by enzymes. The target, in this case, was the synthesis of streptomycin, a marine-derived macrocyclic polyketide that is used as an antibiotic usually employed for the treatment of tuberculosis, obtained through [6 + 4]-cycloadditions.

The goals were to understand the complexity of the transition states of the concerted pericyclic reactions that were proposed in the biosynthetic pathway. Using the CPCM(water)-M06-2X/6-311+G(d,p)//B3LYP-D3/6-31G(d) computational method, they observed an ambimodal character in the enzyme-catalyzed transition state for both cycloadditions, [6 + 4] and [4 + 2], without distinguishing between the *exo* and the *endo* stabilization energies. According to the simulated kinetic data, once the [6 + 4] product (Figure 6c, *i*) is formed, with ca. 23 kcal mol⁻¹ activation Gibbs free energy, it rearranges to the [4 + 2] product (Figure 6c, *ii*) passing through a barrier of ca. 5 kcal mol⁻¹. Alternatively, they identified that this product can be biosynthesized in minor proportion passing by the same 23 kcal mol⁻¹ transition state. In addition, the thermodynamic difference between

Figure 6. (a) Isomerization and oxidation processes in the synthesis of astaxanthin; (b) tautomerization of physalins based on oxa-Michael addition; (c) ambimodal mechanism in cycloaddition of 1,3-diaminocyclohexanetriol. Energy values reported in kcal mol⁻¹.

the [6 + 4] and [4 + 2] products is around 7 kcal mol⁻¹ in favor of the former, with a modest energy preference for the *endo* mechanism.[132]

4. Support to Systems with Environmental Interest

For decades, the scientific community has shown that anthropogenic actions affect the environment and has been warning that containment measures should be taken to stop the climate changes.[133] The increasing industrial development promotes the corresponding high capacity of environmental pollution, leading to a continuous demand to deal with pollutants tossed into nature.[134] The global population is in constant increase, requiring high demand for energy consumption. The primary global energy source comes from fossil fuel burning, which resulted in the rising emission of global greenhouse gases (GHG). According to the Intergovernmental Panel on Climate Change (IPCC) Sixth Assessment Report, even following the Nationally Determined Contributions (NDC) recommendations regarding the emission reduction of GHG, it is still impossible to limit the global warming increase to 1.5 ºC until 2030.[135,136] Thus, the interest in studying environmental systems, beyond repairing anthropogenic impacts but preventing them, increases day by day. In this section, we show several examples that explore reaction mechanisms by computational chemistry to aid environmental issues, such as pollutant gases capture and valorization, pollutants degradation, and energy generation.

The CO₂ emitted to the atmosphere by anthropogenic sources is one of the major causes to the global warming

acceleration.[135] In the last years, the United States, China, and the European Union continued to dominate the global fossil CO₂ emissions, contributing to over 50% of global fossil CO₂ emissions.[133] Much research has been devoted to the design of efficient and sustainable protocols to diminish CO₂ emissions.[137] One way to evaluate the feasibility for the CO₂ capture and valorization is the simulation of reaction mechanisms by molecular modeling.

One of the most widely used strategy to attenuate the negative impact of CO₂ emissions is the post-combustion absorption processes. According to Saeed *et al.*,[138] in the industrial context, aqueous solutions of alkanolamines are the most frequent system to capture CO₂, leading to the production of different compounds, such as carbamates and carbonates, depending on the structural features of the employed alkanolamines. The main representative alkanolamine is monoethanolamine, MEA, due to its ability to remove large volumes of CO₂, high and fast absorption rate, and low cost.[138] The products formed after reacting alkanolamines with CO₂ depends on the structure of the absorbent. MEA produces mainly carbamates in aqueous solution,[139] while *N,N*-disubstituted alkanolamines (tertiary alkanolamines) yield inorganic bicarbonate/carbonate alkanolammonium salts.[137]

dos Santos *et al.*[139] investigated the alkanolamine-promoted CO₂ capture by means of the DFT CAM-B3LYP/6–311++G(2d,2p) method to rationalize how the absorbent system determines the formed products. This method was selected after a comprehensive benchmarking study performed by the same group and has been successfully applied to model the CO₂ capture by different hydroxyl and amine-functionalized substances.[140] The

authors identified by means of ^{13}C NMR and Fourier transform infrared (FTIR) spectroscopies that alkanolamine dimers, present in nonpolar solvent and in pure samples, drive the reaction with CO_2 towards the unexpected carbonate formation (Figure 7a, pathway *i*). However, in 30% (v/v) aqueous solution, carbamates are formed (Figure 7a, pathway *ii*). Computational analysis of the reaction pathways leading to both products indicate that in aqueous media, the alkanolamines react as monomers with CO_2, to form the most stable product, carbamate, releasing enthalpy of 6.8 kcal mol^{-1}. The alternative pathway, formation of carbonates is less exothermic (releasing 2.9 kcal mol^{-1}). In contrast, in nonpolar solvents or pure samples, the alkanolamines react as dimers with CO_2 to produce zwitterionic carbonates with relative enthalpy of -12.7 kcal mol^{-1}, instead of forming carbamates (with relative enthalpy of -5.0 kcal mol^{-1}).[139]

Although being the industrially more used absorbents, the CO_2 capture promoted by aqueous solutions of alkanolamines have several drawbacks, such as formation of thermally stable salts, high energy demands to amine regeneration and water consumption.[141] On the other hand, using nonpolar solvents or pure alkanolamines are environmentally unattractive. Driving the reaction towards carbonates formation instead of carbamates as product requires less energy in the absorbent regeneration step. Hence, the design of new absorbents that lead to carbonate formation is appealing. Although the alcohol function is not nucleophilic enough to react with CO_2, bases could activate the hydroxyl group by hydrogen bonding, making it more reactive towards carbon dioxide.[142,143] Motivated by this hypothesis, Furtado *et al.*[144] combined theoretical and experimental methods to propose ecofriendly and efficient systems to capture CO_2 forming carbonates. Guided by DFT simulations with the IEFPCM(water)-CAM-B3LYP/6-311++G(2d,2p) method, the authors assessed the energetic feasibility of employing different bases with glycerol in the carbonate formation route. The choice for glycerol is attractive, since it is a low cost, biodegradable, eco-friendly, non-toxic and thermally stable solvent. In addition, it is a massive by-product obtained from the biodiesel production process, corresponding to 10-20% of the total volume of biodiesel produced.[145] The simulations indicate that bases of intermediate strength, in the presence of CO_2, can activate glycerol, favoring the formation of the organic carbonate with relative energies in the range of -1.6 to -10 kcal mol^{-1} with respect to the reactants instead of the unwanted carbamates, whose process releases less energy. Figure 7b illustrates both processes. By molecular modeling, the authors were able to suggest that the activation mode of glycerol occurs by

intermolecular hydrogen bonds between primary hydroxyl groups of glycerol and the base, confirmed by both interaction enthalpy (-6.2 kcal mol^{-1}) and by the donor acceptor distance (1.8 Å), increasing its nucleophilicity, and thereby favoring CO_2 capture. Further FTIR and ^{13}C NMR spectroscopies experiments confirmed their expectations, characterizing carbonates as the main products under these conditions.[144]

The examples discussed above show mechanisms for capturing CO_2, which is one of the carbon capture, utilization and storage (CCUS) technologies, that get together strategies to capture more than 95% of the CO_2 emitted in industrial processes.[146] An important pillar of CCUS is the CO_2 utilization processes, in which the captured gas is used as a starting material for a valuable molecule of technological interest.[147] CO_2 is useful in the laboratory and industrial synthesis, once it represents a cheap and abundant C1-building block and can be converted into a series of compounds, such as formic acid, formaldehyde, urea and organic carbonates.[148] The last one is an important class in organic chemistry, being widely used in industry (battery and fuels) and in synthetic processes (solvent and starting material).[148-150] de Andrade *et al.*[151] investigated the reaction mechanism of CO_2 conversion into the simplest organic carbonate: dimethyl carbonate (DMC). They explored the gas capture by methanol catalyzed by tin oxide [Me$_2$SnO]$_2$. The CAM-B3LYP/def2-SVP DFT method was employed together with IEFPCM implicit solvation to simulate the methanol media. The DMC formation passes through three main stages: (*i*) methanol activation, (*ii*) CO_2 capture, and (*iii*) DMC formation (Figure 7c). In the first step, the catalyst [(Me)$_2$SnO]$_2$ **1** activates the methanol and forms the effective capture agent [(Me)$_2$Sn(OMe)$_2$]$_2$ **2**, in an exothermic processes with low activation energy ($\Delta H^{\ddagger} < 9$ kcal mol^{-1}). Next, two CO_2 molecules are captured by the oxide dimer with energy barriers around 5 kcal mol^{-1} and releasing ca. 13 kcal mol^{-1}, forming the key intermediate tin carbonate **3**. As the key intermediate is a dimer, the authors expected the formation of two DMC molecules *per* carbonate site. They identified the formation only of the first DMC by intramolecular processes (rds $\Delta H^{\ddagger} = 25.7$ kcal mol^{-1}). The final DMC molecule arises from the hemicarbonate (**4**) dimerization, assisted by one methanol molecule, with a simulated high energy barrier (about 30 kcal mol^{-1}). This mechanistic proposal agrees with structure characterization experiments that identified the existence of the tin compounds **4** and **5**.[152,153] Despite the complete DMC formation, the initial catalyst, (Me)$_2$Sn(OMe)$_2$, is not regenerated in the system. Instead, the final organotin compound is (Me)$_2$OH(Sn)OOMe(Sn)(Me)$_2$ dimer **5**.[151] These computational results agreed with

experimental identification that DMC formation from tin carbonate intermediate is a thermolysis step, that is, needs high energy (as calculated by de Andrade *et al.*[151]).[154]

The global energy supply, as well as CO_2 emission into the atmosphere, consists largely in fossil fuel burning, with petroleum being the most utilized source. When extracted from the reservoir, the crude oil contains sulfur and nitrogen compounds, considered impurities, granting the oil undesired characteristics.[155] Sulfur, after carbon and hydrogen, is the most abundant element in petroleum. The removal of sulfur compounds usually occurs in hydrodesulfurization (HDS) processes during the refinement of petroleum, which produces hydrogen sulfur (H_2S). This is an acid colorless gas and stands as one of the main problems related to the petroleum industry, because of its alarming toxicity, corrosiveness, pollutant character, and fouling activity. Thus, many H_2S scavengers have been developed to extend the lifetime of installations and guarantee better safety and health conditions to the workers.[156-158] The class of hexahydro-1,3,5-triazines stand out as one of the most frequent non-regenerative scavengers, because of its favorable kinetic profile. They quickly react with H_2S, reducing the concentrations from 100 ppm down to 5 ppm. The most representative hexahydro-1,3,5-triazines is the 1,3,5-tris(2-hydroxyethyl)hexahydro-*s*-triazine, HET, due to its remarkable biodegradability, low toxicity and high water-solubility.[157] Despite of being widely employed by the petroleum industry, until recently,[159] there was a lack of information regarding the supposed S_N2 mechanism and its thermodynamic and kinetic profile. In their pioneer work, Fiorot and Carneiro[159] explored the reaction pathway for H_2S scavenge by the triazine, by means of computational chemistry at the CAM-B3LYP/6-311++G(2d,2p) level to explain the unexpected stoichiometric ratio of 2:1 (H_2S:HET), even though the 3:1 ratio might be supposed, since three reactant sites are available to react with H_2S. The calculations suggested that for the first H_2S equivalent scavenged, the mechanism follows preferentially a S_N1 pathway, since the energy to form the carbocation ($\Delta H = 14.6$ kcal mol^{-1}) is lower than the energy barrier for the respective S_N2 concerted TS ($\Delta H^{\ddagger} = 18.3$ kcal mol^{-1}). For the second equivalent of H_2S, the S_N1 and S_N2 pathways are competitive, as the energy required to form the carbocation (S_N1) is almost the same as that required to overcome the barrier height concerning the S_N2 pathway (ca. 20 kcal mol^{-1} in terms of enthalpy). The capture of the third equivalent of H_2S is prohibitive due to kinetic reasons, since the energy barrier associated with the process is approximately 40 kcal mol^{-1}. The authors correlated the energy barrier values with the nature of the electrophilic carbon: when it is bonded to two nitrogen atoms (electrophilic carbon

indicated with the red index a in Figure 7d), the barrier is lower than 24 kcal mol^{-1}, thus the process is feasible at the conditions at which the H_2S is scavenged. However, when a sulfur atom is bonded to the electrophilic carbon (indicated by the index b, Figure 7d), the barrier increases to ca. 40 kcal mol^{-1}, impeding the reaction to occur.[159] With these results, the authors justified why hexahydro-1,3,5-triazines are able to capture only two equivalents of H_2S, and not three, as might be supposed on the bases of the number of nitrogen atom in the triazine molecule.[159]

Environmental pollution and energy demand has continuously increased over the past century. Photocatalysis shows high efficiency, non-secondary pollution and low energy consumption. For those reasons, photocatalysis is a sustainable strategy to address environmental pollution and degrading organic pollutants.[160,161] Graphitic carbon nitride (g-C_3N_4) has become an attractive organic semiconductor in photocatalysis because of its thermal and chemical stability, suitable optical band gap (approx. 2.7 eV), low cost and ecofriendly character. However, g-C_3N_4 shows inferior mobility of photoexcited charge carriers, as well as poor specific surface area, leading to inferior photocatalytic activity. Hence, several studies[162,163] have shown that heteroatoms doping enhances the photocatalytic performance of g-C_3N_4.

Zhang *et al.*[161] employed the DFT Vienna *ab initio* Simulation Package (VASP) to investigate the mechanism of enhanced photodegradation of toxic organic pollutants and to explore optimal oxygen-doping positions. They replaced the N atoms by O atoms in the g-C_3N_4 and compared their formation energies, assuming that lower values correspond to better doping positions. The calculations revealed a formation energy value of –2.66 eV at both N1' and N4' sites. DFT calculations combined with experimental data have shown that O-doping leads to an effective charge transfer and separation of dual-oxygen-doped porous g-C_3N_4 (OPCN) by forming conjugate systems of surface e$^-$ and h$^+$ (the resulting system after the radiation), under visible light irradiation, that benefited its interfacial contact with organic pollutants and adsorbed O_2. Thus, the authors stated that doping nonmetallic elements of g-C_3N_4 with stronger electronegativity than carbon provides a hopeful approach for highly effective nonmetal photocatalysts production.[161]

Besides of using electromagnetic radiation to decompose organic pollutants in photodegradation processes as just exemplified, the light, by being the cleanest energy source, is an attractive alternative to diminish fossil fuel consumption (currently over than 11.000 MtOE *per* year).[164] Molecular solar thermal energy storage (MOST) emerged as a promising technology to convert and store light into thermal energy by means of molecular photoswitches.
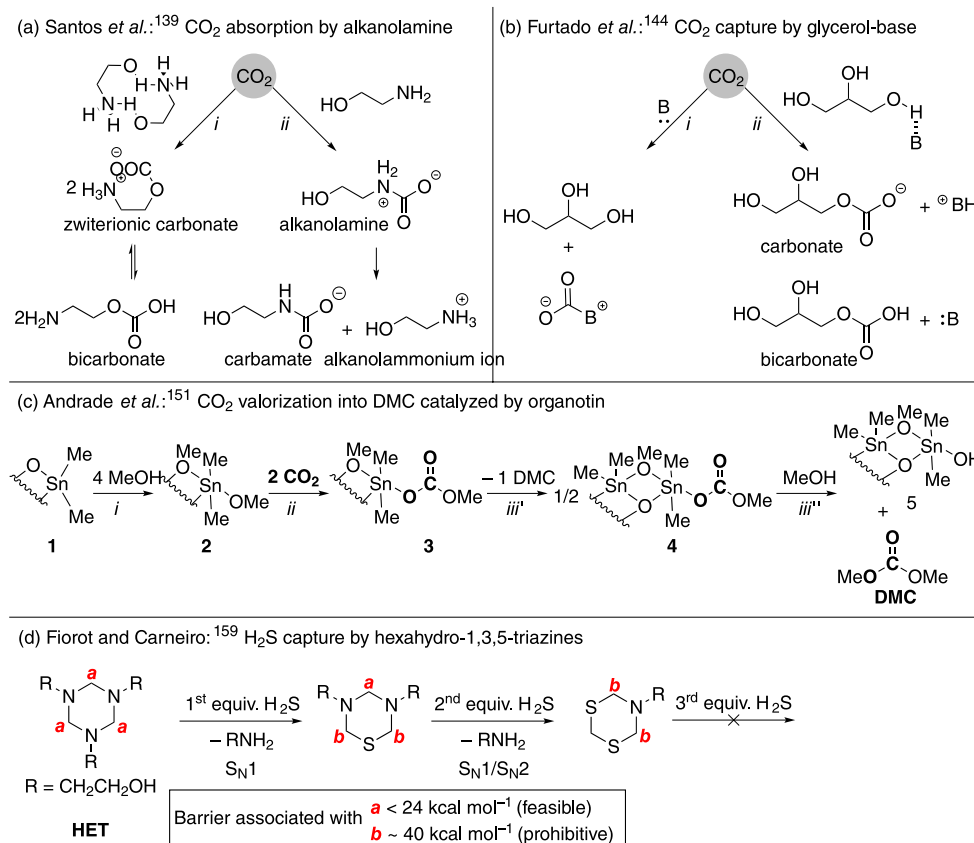
Figure 7. (a) Reaction scheme for CO_2 absorption by alkanolamine dimers (*i*) and monomers (*ii*); (b) CO_2 capture by the system glycerol-base and product formation highlights; (c) relevant steps for CO_2 conversion into DMC promoted by methanol and tin oxide. The structures represent only one unit of the dimer; (d) H_2S scavenging activity of hexahydro-1,3,5-triazines.

These compounds undergo reversible photoinducted modifications, such as isomerization, by absorbing and storing solar energy to release it as heat on demand.[164] Examples of interesting molecular systems are the azobenzenes (AZO), that, according to Kolpak and Grossman,[165] undertake an *E-Z* isomerization in the presence of irradiation, storing $\Delta H = 1.55$ eV *per* azobenzene[163] (Figure 8a), and norbornadienes (NBD) that undergoes a [2 + 2] cycloaddition to form quadricyclanes (QC) (Figure 8b).[164,166]

Wang *et al.*[167] assessed the macroscopic heat release in a system constituted by a switchable norbornadiene (NBD)-quadricyclane (QC) couple (Figure 8b), referred as a promising candidate for MOST applications. For the photoisomerization process (a [2 + 2]-cycloaddition reaction), they identified a quantum yield of 61% to convert the NBD into the metastable QC form, indicating that most of the absorbed photons are involved in the photoconversion. For a system to work as a MOST, the metastable form obtained after the photoabsorption should have a long half-life time ($t_{1/2}$). In this case, they calculated a long half-time life of 30 days at 25 °C, demonstrating to be stable under ambient conditions. To trigger the heat

release, they evaluated the QC→NBD back-conversion catalyzed by a cobalt phthalocyanine physisorbed on an activated carbon support (CoPc@C). The authors showed by differential scanning calorimetry (DSC) experiments that for a solution of 1.5 M of QC1, the temperature rapidly rises ($\Delta T = 63.4$ °C) in only 2.5 min, corresponding to a $\Delta H_{storage} = 21.2$ kcal mol^{-1}, highlighting the efficiency of heat release over a short time. To understand this rapid heat release at a molecular level, the authors carried out simulations at the M06/6-31+G* level for the CoPc@C-catalyzed QC conversion into NBD. They assessed different pathways, since QC has four C–C labile bonds able to the oxidative addition to the metal center of CoPc@C (Figure 8b). The substituents (*p*-methoxyphenyl and cyano) control the order of which C–C bond adds to the Co and, thus, the barrier height values, mostly because of positive-charge stabilization. These computational outcomes are consistent to two important experimental observations: (*i*) the energy difference between the NBD and QC, –19.9 kcal mol^{-1} (corresponding to a temperature elevation of $\Delta T = 61.7$ °C), is in good agreement with the experimental value of 63.4 °C considering the limit of the DSC equipment; (*ii*) the computed low energy barriers for

the preferred reaction pathway (approx. 12 kcal mol^{-1}) is compatible with the rapid heat release in the QC→NBD back-conversion.[167]

Another molecular system based on the NBD-QC couple is the biclyclooctadienes (BODs) - tetracyclooctanes (TCOs), which has its MOST properties less explored. Although TCO has promising energy storage capacity, its rapid retro-conversion to BOD through thermal activation processes causes it to have a short half-life time. Besides that, the BOD synthesis is not a trivial task, once this compound is degraded under high temperatures via a retro-Diels-Alder process (Figure 8c, RDA).[66] Quant *et al.*[168] overcame such limitations from the experimental-

(a) Kolpak and Grossman:[165] AZO isomerization

(b) Wang *et al.*:[167] QC catalytic conversion to NBD

(c) Quant *et al.*:[168] BOD-TCO system and competitive product
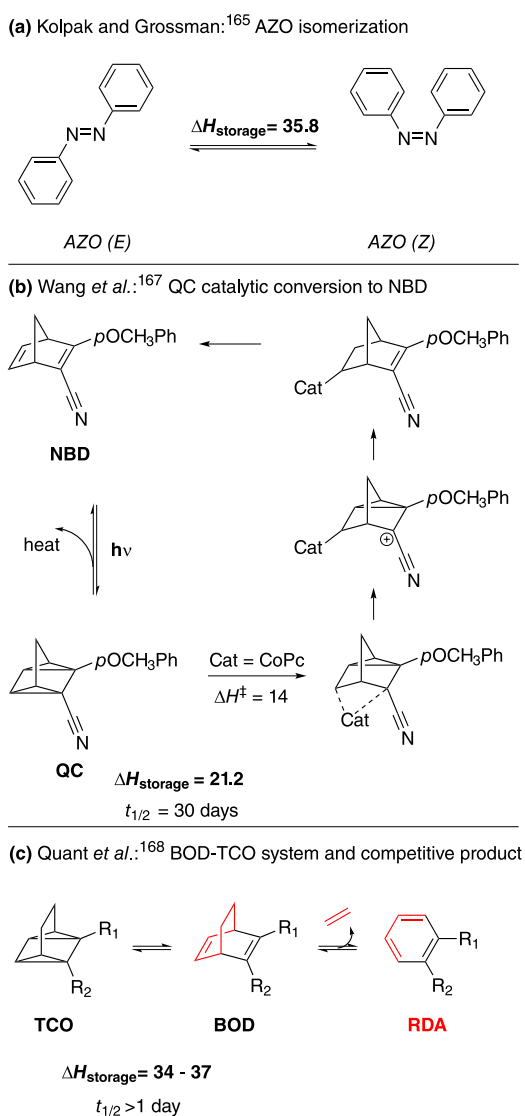
Figure 8. (a) *E-Z* isomerization of azobenzenes (AZO) compounds in presence of irradiation; (b) relevant stationary points of catalytic (CoPc) conversion of QC to initial compound NBD; (c) possibility of BOD conversion to TCO (energy storage and MOST applicability) and RDA (thermal degradation via retro-Diels-Alder reaction). Energy values reported in kcal mol^{-1}.

computational combination in the evaluation of this system for the MOST applications. They identified an alternative synthetic method for the Diels-Alder reaction using cross-coupling reactions, avoiding its thermal degradation, while the TCO half-life time was optimized from the inclusion of electron density donor substituents. From computational perspective, they employed the DFT M06-2X/6-311++G(d,p) level of theory to assess the energy storage and the reaction barriers for the BOD→TCO conversion. For all the BOD-TCO systems, the calculated storage energies ranged from 34 to 37 kcal mol^{-1}, being 49-76% higher than the NBD-QC couple. Besides the target reaction (BOD→TCO), the authors also evaluated the competitive product of BOD degradation from the retro-Diels-Alder process. From the design of several substituents at the R_1 and R_2 positions, they identified that the substituent by R_1 = COOEt and R_2 = *p*-PhOMe favors the TCO pathway rather than the RDA competitive product by $\Delta\Delta G^{\ddagger}$ = 9 kcal mol^{-1}. Even the DFT evaluations pointed out that only for that combination there is no formation of RDA. Experimental evaluation of BOD thermal stability (75 °C, 1 h) showed by NMR analysis that there is no degradation for all systems. The authors ascribed that to limitations associated with the level of theory (M06-2X).[168]

5. Final Remarks

With the advent of the computational chemistry and continuous software and hardware development, the exploration of chemical transformations and their mechanisms by molecular simulations turned to be a common task. Nowadays, this is a well-established area in chemistry and one of its main pillars, alongside with synthesis and spectroscopy. Scientific communities from different areas have been taking advantage of these technologies to computationally-aid their matters, whether by designing chemical processes and predicting important properties or by rationalizing some intriguing experimental observation. In this perspective, we highlighted some important applications of how molecular simulations can be useful to tackle issues from organic synthesis, natural products chemistry and systems of environmental interest. We selected some examples that show successful interplay between theory and experiment, bringing some of our particular experience.

Herein, we showed that the computational support help understanding the selectivity (stereo-, regio-, or chemo-) of a given reaction, computing kinetics and thermodynamics descriptors of the processes and mapping the reaction mechanism for different species. In particular, the use of explicit solvation (microsolvation), usually together with

an implicit model (hybrid method) provides significant results on the effect of the solvent on the reaction medium. The theory-experiment synergy has also proved to be essential in advancing research in the chemistry of natural products and environmental issues, making it possible to assist in the mitigation of anthropogenic impacts. Several tools have been developed, which open the fields to further and deeper exploration, including machine learning, data augmentation, and automation. Although we are experiencing a fast development of computers and methods to approach physical and chemical problems, there are some bottlenecks associated mainly with the computational resource limitation. This makes the development of more efficient simulation technologies a constantly growing field, with the great ambition of more complex molecular modeling research, such as the exploration of reaction mechanisms in several stages, enzyme design, and new synthetic methodologies.[169]

Acknowledgments

Author Contributions

Karine N. de Andrade was responsible for conceptualization, data curation, writing original draft and editing; José Renato D. Fajardo for data curation, writing original draft; Caio A. Leal for data curation, writing original draft; José Walkimar de M. Carneiro for conceptualization, visualization, writing-review and editing; Rodolfo G. Fiorot for conceptualization, project administration, resources, funding acquisition, writing original draft, writing-review and editing.

Karine Nascimento de Andrade has bachelor's degree (2018) and master's in Chemistry (2021) from Universidade Federal Fluminense (2018). Currently, she is a doctoral student at the same university. She has experience in the field of Chemistry, with emphasis on Physical Organic Chemistry and Molecular Modeling, working on the following topics: Density Functional Theory, Reactional Mechanisms, Explicit Solvation, Carbon Capture and Utilization, and photoresponsive molecular technologies.

José Renato Duarte Fajardo is in the final year of pharmacy bachelor from Universidade Federal Fluminense, bound to a scholarship by CNPq since 2020. He is a freshman in academia with a line of research in Chemistry, focusing on Computational Chemistry and its applications in the most diverse fields.

Caio Astigarreta Leal undergoing master's degree in computational chemistry and graduated in Chemistry at the Universidade Federal Fluminense (UFF), with experience in organic synthesis. Currently, he is part of the research group in computational chemistry of Structure and Reactivity of Organic Compounds (ERCO), also at UFF, studying H_2S scavenger capacity of aldehydes using the Density Functional Theory.

José Walkimar de Mesquita Carneiro is graduated in Industrial Chemistry from UFMA, with a master's and doctorate in Chemistry from IME-RJ. He joined the Fluminense Federal University in 1992, currently holding the position of Full Professor. He has been a CNPq fellow since the 1990s and has been a Scientist of Our State by FAPERJ on four occasions. Consultant for the main Brazilian development agencies and editor of the Journal of the Brazilian Chemical Society. Recently, he received the Walter Mors Medal from SBQ-Rio and the Scientific Excellence Award from Universidade Federal Fluminense. He has experience in Computational Chemistry, with an emphasis on Organic Physical Chemistry and Inorganic Physical Chemistry.

Rodolfo Goetze Fiorot is Professor in the Organic Chemistry Department at the Universidade Federal Fluminense (UFF-RJ) since 2020. He earned his BSc (2013) and his MSc (2015) in Chemistry working with the synthesis of bioactive organic compounds at the Universidade Federal do Espírito Santo. In 2019, he received his PhD in Chemistry at UFF-RJ investigating reaction mechanisms of organic transformations and systems with environmental interest by Computational Chemistry. His research expertise and interests include the computational evaluations of the

Structure and Reactivity of Organic Compounds, and the rational design of molecular materials.

References

1. Nicolaou, K. C.; *Proc. R. Soc. A* **2014**, *470*, 20130690. [Crossref]

2. IUPAC; *Compendium of Chemical Terminology: Reaction Mechanisms*, 2ⁿᵈ ed.; Blackwell Scientific Publications: Oxford, UK, 1997. [Crossref]

3. Nelson, D. L.; Cox, M. M.; *Lehninger Principles of Biochemistry*, 4ᵗʰ ed.; W. H. Freeman: New York, USA, 2005.

4. Vollhardt, K. P. C.; Shore, N. E.; *Organic Chemistry: Structure and Function*, 3ʳᵈ ed.; W. H. Freeman: New York, USA, 1999, p. 5.

5. Espenson, J. H.; *Chemical Kinetics and Reaction Mechanisms*, 2ⁿᵈ ed.; McGraw-Hill: New York, USA, 1995.

6. Anslyn, E. V.; Dougherty, D. A.; *Modern Physical Organic Chemistry*; University Science Books: Sausalito, CA, 2006.

7. Buskirk, A.; Baradaran, H.; *J. Chem. Educ.* **2009**, *86*, 551. [Crossref]

8. Scott, S. L.; *ACS Catal.* **2019**, *9*, 4706. [Crossref]

9. Karthikeyan, A.; Priyakumar, U. D.; *J. Chem. Sci.* **2022**, *134*, 2. [Crossref]

10. Costa, F. L. P.; de Albuquerque, A. C. F.; Fiorot, R. G.; Lião, L. M.; Martorano, L. H.; Mota, G. V. S.; Valverde, A. L.; Carneiro, J. W. M.; dos Santos Jr., F. M.; *Org. Chem. Front.* **2021**, *8*, 2019. [Crossref]

11. Cheng, G.-J.; Zhang, X.; Chung, L. W.; Xu, L.; Wu, Y.-D.; *J. Am. Chem. Soc.* **2015**, *137*, 1706. [Crossref]

12. Lan, J.; Li, X.; Yang, Y.; Zhang, X.; Chung, L. W.; *Acc. Chem. Res.* **2022**, *55*, 1109. [Crossref]

13. Ahn, S.; Hong, M.; Sundararajan, M.; Ess, D. H.; Baik, M.-H.; *Chem. Rev.* **2019**, *119*, 6509. [Crossref]

14. Seybold, P. G.; Shields, G. C.; *WIREs Comput. Mol. Sci.* **2015**, *5*, 290. [Crossref]

15. Chin, Y. P.; See, N. W.; Jenkins, I. D.; Krenske, E. H.; *Org. Biomol. Chem.* **2022**, *20*, 2028. [Crossref]

16. Schlegel, H. B.; *J. Comput. Chem.* **2003**, *24*, 1514. [Crossref]

17. Cramer, C. J.; *Essentials of Computational Chemistry. Theory and Models*, 2ⁿᵈ ed.; John Wiley & Sons: Chichester, UK, 2004.

18. Roothaan, C. C. J.; *Rev. Mod. Phys.* **1951**, *23*, 69. [Crossref]

19. Goddard, W. A.; Dunning, T. H.; Hunt, W. J.; Hay, P. J.; *Acc. Chem. Res.* **1973**, *6*, 368. [Crossref]

20. Goodgame, M. M.; Goddard, W. A.; *Phys. Rev. Lett.* **1985**, *54*, 661. [Crossref]

21. Krishman, R.; Schlegel, H. B.; Pople, J. A.; *J. Chem. Phys.* **1980**, *72*, 4654. [Crossref]

22. Krishman, R.; Pople, J.; *Int. J. Quantum Chem.* **1981**, *20*, 1067. [Crossref]

23. Buenker, R. J.; Peyerimhoff, S. D.; Butscher, W.; *Mol. Phys.* **1978**, *35*, 771. [Crossref]

24. Werner, H.; Knowles, P. J.; *J. Chem. Phys.* **1988**, *89*, 5803. [Crossref]

25. Andersson, K.; Malmqvist, P. A.; Ross, B. O.; Sadlej, A. J.; Wolinski, K.; *J. Phys. Chem.* **1990**, *94*, 5483. [Crossref]

26. Andersson, K.; Malmqvist, P. A.; Ross, B. O.; *J. Chem. Phys.* **1992**, *96*, 1218. [Crossref]

27. Hohenberg, P.; Kohn, W.; *Phys. Rev.* **1964**, *136*, 864. [Crossref]

28. Kohn, W.; Sham, L. J.; *Phys. Rev.* **1965**, *140*, 1133. [Crossref]

29. Parr, R. G.; Yang, W.; *Density-Functional Theory of Atoms and Molecules*; Oxford University Press: Oxford, 1989.

30. Wagner, J. P.; Schreiner, P. R.; *Angew. Chem., Int. Ed.* **2015**, *54*, 12274. [Crossref]

31. Grimme, S.; *WIREs Comput. Mol. Sci.* **2011**, *1*, 211. [Crossref]

32. Otero-de-la-Roza, A.; Johnson, R.; *J. Chem. Phys.* **2012**, *136*, 174109. [Crossref]

33. Grimme, S.; Hansen, A.; Brandenburg, J. G.; Bannwarth, C.; *Chem. Rev.* **2016**, *116*, 5105. [Crossref]

34. Schreiner, P. R.; Chernish, L. V.; Gunchenko, P. A.; Tikhonchuk, E. Y.; Hausmann, H.; Serafin, M.; Schlecht, S.; Dahl, J. E. P.; Carlson, R. M. K.; Fokin, A. A.; *Nature* **2011**, *477*, 308. [Crossref]

35. Delgado, A. A. A.; Humanson, A.; Kalescky, R.; Freindorf, M.; Kraka, E.; *Molecules* **2021**, *26*, 950. [Crossref]

36. Kubo, T.; Suga, Y.; Hashizume, D.; Suzuki, H.; Miyamoto, T.; Okamoto, H.; Kishi, R.; Nakano, M.; *J. Am. Chem. Soc.* **2021**, *143*, 14360. [Crossref]

37. Osuna, S.; Swart, M.; Solà, M.; *J. Phys. Chem. A* **2011**, *115*, 3491. [Crossref]

38. Aikawa, H.; Takahira, Y.; Yamaguchi, M.; *Chem. Comm.* **2011**, *47*, 1479. [Crossref]

39. Bursch, M.; Caldeweyher, E.; Hansen, A.; Neugebauer, H.; Ehlert, S.; Grimme, S.; *Acc. Chem. Res.* **2019**, *52*, 258. [Crossref]

40. Grimme, S.; *J. Comput. Chem.* **2006**, *27*, 1787. [Crossref]

41. Grimme, S.; Antony, J.; Ehrlich, S.; Krieg, H.; *J. Chem. Phys.* **2010**, *132*, 154104. [Crossref]

42. Grimme, S.; Ehrlich, S.; Goerigk, L.; *J. Comput. Chem.* **2011**, *32*, 1456. [Crossref]

43. Caldeweyher, E.; Mewes, J.-M.; Ehlert, S.; Grimme, S.; *Phys. Chem. Chem. Phys.* **2020**, *22*, 8499. [Crossref]

44. Caldeweyher, E.; Ehlert, S.; Hansen, A.; Neugebauer, H.; Spicher, S.; Bannwarth, C.; Grimme, S.; *J. Chem. Phys.* **2019**, *150*, 154122. [Crossref]

45. Ess, D. H.; Houk, K. N.; *J. Am. Chem. Soc.* **2007**, *129*, 10646. [Crossref]

46. Fernández, I.; Bickelhaupt, M.; *Chem. Soc. Rev.* **2014**, *43*, 4953. [Crossref]

47. Kitaura, K.; Morokuma, K.; *Int. J. Quantum Chem.* **1976**, *10*, 325. [Crossref]

48. Frenking, G.; Bickelhaupt, F. M. In *The Chemical Bond*; Frenking, G.; Shaik, S., eds.; John Wiley & Sons: Chichester, UK, 2014, p. 121.

49. Ziegler, T.; Rauk, A.; *Inorg. Chem.* **1979**, *18*, 1558. [Crossref]

50. Bickelhaupt, F. M.; *J. Comp. Chem.* **1999**, *20*, 114. [Crossref]

51. Wolters, L. P.; Bickelhaupt, F. M.; *WIREs Comput. Mol. Sci.* **2015**, *5*, 324. [Crossref]

52. Bickelhaupt, F. M.; Houk, K. N.; *Angew. Chem., Int. Ed.* **2017**, *56*, 10070. [Crossref]

53. Vermeeren, P.; van der Lubbe, S. C. C.; Guerra, C. F.; Bickelhaupt, F. M.; Hamlin, T. A.; *Nat. Protoc.* **2020**, *15*, 649. [Crossref]

54. Johnson, E. R.; Keinan, S.; Mori-Sánchez, P.; Contreras-García, J.; Cohen, A. J.; Yang, W.; *J. Am. Chem. Soc.* **2010**, *132*, 6498. [Crossref]

55. Boto, R. A.; Peccati, F.; Laplaza, R.; Quan, C.; Carbone, A.; Piquemal J.-P.; Maday, Y.; Contreras-García, J.; *J. Chem. Theory Comput.* **2020**, *16*, 4150. [Crossref]

56. Contreras-García, J.; Johnson, E. R.; Keinan, S.; Chaudret, R.; Piquemal, J.-P.; Beratan, D. N.; Yang, W.; *J. Chem. Theory Comput.* **2011**, *7*, 625. [Crossref]

57. Laplaza, R.; Peccati, F.; Boto, R. A.; Quan, C.; Carbone, A.; Piquemal, J.-P.; Contreras-García, J.; *WIREs Comput. Mol. Sci.* **2021**, *11*, e1497. [Crossref]

58. Pilme, J.; Renault, E.; Bassal, F.; Amaouch, M.; Montavon, G.; Galland, N.; *J. Chem. Theory Comput.* **2014**, *10*, 4830. [Crossref]

59. Bader, R. F. W.; Beddall, P. M.; *J. Am. Chem. Soc.* **1973**, *95*, 305. [Crossref]

60. Bader, R. F. W.; *Atoms in Molecules: A Quantum Theory*; Oxford University Press: New York, 1994.

61. Glendening, E. D.; Landis, C. R.; Weinhold, F.; *WIREs Comput. Mol. Sci.* **2012**, *2*, 1. [Crossref]

62. Weinhold, F.; Landis, C. R.; *Valency and Bonding: A Natural Bond Orbital Donor-Acceptor Perspective*; Cambridge University Press: Cambridge, 2005.

63. Cramer, C. J.; Truhlar, D. G.; *Chem. Rev.* **1999**, *99*, 2161. [Crossref]

64. Zhang, J.; Zhang, H.; Wu, T.; Wang, Q.; van der Spoel, D.; *J. Chem. Theory Comput.* **2017**, *13*, 1034. [Crossref]

65. Steiner, M.; Holzknecht, T.; Schauperl, M.; Podewitz, M.; *Molecules* **2021**, *26*, 1793. [Crossref]

66. Pliego Jr., J. R.; Riveros, J. M.; *WIREs Comput. Mol. Sci.* **2020**, *10*, e1440. [Crossref]

67. Ahmadi, S.; Herrera, L. B.; Chehelamirani, M.; Hostas, J.; Jalife, S.; Salahub, D. R.; *Int. J. Quantum Chem.* **2018**, *118*, e25558. [Crossref]

68. Vreven, T.; Morokuma, K.; *Annu. Rep. Comput. Chem.* **2006**, *2*, 35. [Crossref]

69. Lipparini, F.; Mennucci, B.; *Chem. Phys. Rev.* **2021**, *2*, 041303. [Crossref]

70. Fianchini, M.; *Phys. Sci. Rev.* **2017**, *2*, 20170134. [Crossref]

71. Nogueira, I. C.; Pliego Jr., J. R.; *J. Braz. Chem. Soc.* **2023**, *34*, 194. [Crossref]

72. Hamlin, T. A.; Swart, M.; Bickelhaupt, F. M.; *ChemPhysChem* **2018**, *19*, 1315. [Crossref]

73. Varejão, J. O. S.; Barbosa, L. C. A.; Varejão, E. V. V.; Souza, A. H.; Lage, M. R.; Carneiro, J. W. M.; *J. Braz. Chem. Soc.* **2020**, *31*, 90. [Crossref]

74. Esquivel, E. C. C.; Rufino, V. C.; Nogueira, M. H. T.; Souza, A. C. C.; Pliego Jr., J. R.; Valle, M. S.; *J. Mol. Struct.* **2020**, *1204*, 127536. [Crossref]

75. Shang, F.; Liu, J.; Zhou, P.; Zhang, C.; *Tetrahedron* **2021**, *77*, 131737. [Crossref]

76. Kunikazu, S.; Nobuko, H.; Kiyosi, K.; *Bull. Chem. Soc. Jpn.* **1986**, *59*, 179. [Crossref]

77. Hanselmann, R.; Job, G. E.; Johnson, G.; Lou, R.; Martynow, J. G.; Reeve, M. M.; *Org. Process Res. Dev.* **2010**, *14*, 152. [Crossref]

78. van der Helm, M. P.; Klemm, B.; Eelkema, R.; *Nat. Rev. Chem.* **2019**, *3*, 491. [Crossref]

79. Cândido, A. A.; Rozada, T. C.; Rozada, A. M. F.; Souza, J. R. B.; Pilau, E. J.; Rosa, F. A.; Basso, E. A.; Gauze, G. F.; *J. Braz. Chem. Soc.* **2020**, *31*, 1796. [Crossref]

80. Flanigan, D. M.; Romanov-Michailidis, F.; White, N. A.; Rovis, T.; *Chem. Rev.* **2015**, *17*, 9307. [Crossref]

81. Barik, S.; Biju, A. T.; *Chem. Commun.* **2020**, *56*, 15484. [Crossref]

82. Narayana, Y.; N. C., S.; Dinesh, H.; Thimmaiah, S. B.; Rangappa, K. S.; Mantelingu, K. In *Carbene: N-Heterocyclic Carbene Mediated Organocatalysis Reactions*, 1st ed.; Saha, S.; Manna, A., eds.; IntechOpen: London, UK, 2021. [Crossref]

83. Labet, M.; Thielemans, W.; *Chem. Soc. Rev.* **2009**, *38*, 3484. [Crossref]

84. Lessa, M. D.; Fajardo, J. R. D.; Delarmelina, M.; Carneiro, J. W. M.; *Mol. Catal.* **2021**, *515*, 111896. [Crossref]

85. Jones, G. O.; Chang, Y. A.; Horn, H. W.; Acharya, A. K.; Rice, J. E.; Hedrick, J. L.; Waymouth, R. M.; *J. Phys. Chem. B* **2015**, *17*, 5728. [Crossref]

86. MacMillan, D. W. C.; *Nature* **2008**, *455*, 304. [Crossref]

87. Seayad, J.; List, B.; *Org. Biomol. Chem.* **2005**, *3*, 719. [Crossref]

88. List, B.; *Nobel Prize Lecture: Asymmetric Organocatalysis*, https://www.nobelprize.org/prizes/chemistry/2021/list/lecture/, accessed in March 2023.

89. MacMillan, D. W. C.; *Nobel Prize Lecture: Democratizing Catalysis for a Sustainable World*, https://www.nobelprize.org/prizes/chemistry/2021/macmillan/lecture, accessed in March 2023.

90. He, C.; Zhou, Y.; Li, Z.; Xu, J.; Chen, X.; *Org. Chem. Front.* **2021**, *8*, 1569. [Crossref]

91. Li, Y.; Song, Z.; Zhang, Z.; *Mol. Catal.* **2022**, *524*, 112311. [Crossref]

92. Palazzo, T. A.; Mose, R.; Jorgensen, K. A.; *Angew. Chem., Int. Ed.* **2017**, *56*, 10033. [Crossref]

93. Chen, Y.; Ling, J.; Keto, A. B.; He, Y.; Low, K.-H.; Krenske, E. H.; Chiu, P.; *Angew. Chem., Int. Ed.* **2022**, *61*, e202116099. [Crossref]

94. Chung, W. K.; Lam, S. K.; Lo, B.; Liu, L. L.; Wong, W.; Chiu, P.; *J. Am. Chem. Soc.* **2009**, *131*, 4556. [Crossref]

95. Alnajjar, R. A.; Jasinski, R.; *J. Mol. Model.* **2019**, *25*, 157. [Crossref]

96. Fiorot, R. G.; Vilhena, F. S.; Carneiro, J. W. M.; *J. Mol. Model.* **2019**, *25*, 306. [Crossref]

97. Pahn, T. B.; Nolte, C.; Kobayashi, S.; Ofial, A. R.; Mary, H.; *J. Am. Chem. Soc.* **2009**, *32*, 11392. [Crossref]

98. Carey, F. A.; *Advanced Organic Chemistry*, 5th ed.; Plenum Press: New York, USA, 2010.

99. Bento, A. P.; Bickelhaupt, F. M.; *Chem. Asian J.* **2008**, *3*, 1783. [Crossref]

100. Evangelista, T. C. S.; Delarmelina, M.; Addla, D.; Allão, R. A.; Kaiser, C. R.; Carneiro, J. W. M.; Silva-Jr., F. P.; Ferreira, S. B.; *Tetrahedron Lett.* **2021**, *68*, 152937. [Crossref]

101. Batalha, P. N.; Forezi, L. S. M.; Freitas, M. C. R.; Tolentino, N. M. C.; Orestes, E.; Carneiro, J. W. M.; Boechat, F. C. S.; de Souza, M. C. B. V.; *Beilstein J. Org. Chem.* **2019**, *15*, 388. [Crossref]

102. Delarmelina, M.; Ferreira, S. B.; da Silva, F. C.; Ferreira, V. F.; Carneiro, J. W. M.; *J. Org. Chem.* **2020**, *85*, 7001. [Crossref]

103. Hansen, T.; Roozee, J. C.; Bickelhaupt, F. M.; Hamlin, T. A.; *J. Org. Chem.* **2022**, *87*, 1805. [Crossref]

104. Tomasi, J.; Mennucci, B.; Cammi, R.; *Chem. Rev.* **2005**, *105*, 2999. [Crossref]

105. Simm, G. N.; Turtscher, P. L.; Reiher, M.; *J. Comp. Chem.* **2020**, *41*, 1144. [Crossref]

106. Delarmelina, M.; Nicoletti, C. D.; Moraes, M. C.; Futuro, D. O.; Bühl, M.; Silva, F. C.; Ferreira, V. F.; Carneiro, J. W. M.; *ChemPlusChem* **2019**, *84*, 52. [Crossref]

107. Fiorot, R. G.; Rambabu, G.; Vijayakumar, V.; Kiran, Y. B.; Carneiro, J. W. M.; *J. Braz. Chem. Soc.* **2019**, *30*, 1717. [Crossref]

108. Yamabe, S.; Fukuda, T.; Yamazaki, S.; *Beilstein J. Org. Chem.* **2013**, *9*, 476. [Crossref]

109. Lisboa, F. M.; Pliego Jr., J. R.; *J. Mol. Model.* **2022**, *28*, 159. [Crossref]

110. Sousa-Herves, A.; Wedepohl, S.; Calderón, M.; *Chem. Commun.* **2015**, *51*, 5264. [Crossref]

111. Tantillo, D. J.; *Applied Theoretical Organic Chemistry*; World Scientific: Europe, 2018. [Crossref]

112. Tantillo, D. J.; *Chem. Soc. Rev.* **2018**, *47*, 7845. [Crossref]

113. Wang, Z.; Zhao, W.; Hao, G.; Song, B.; *Org. Chem. Front.* **2021**, *8*, 812. [Crossref]

114. Batista, A. N. L.; Angrisani, B. R. P.; Lima, M. E. D.; da Silva, S. M. P.; Schettini, V. H.; Chagas, H. A.; dos Santos Jr., F. M.;

115. Batista Jr., J. M.; Valverde, A. L.; *J. Braz. Chem. Soc.* **2021**, *32*, 1499. [Crossref]

116. Nicolaou, K. C.; Snyder, S. A.; *Angew. Chem., Int. Ed.* **2005**, *44*, 1012. [Crossref]

117. Tantillo, D. J.; *WIREs Comp. Mol. Sci.* **2020**, *10*, e1453. [Crossref]

118. Martorano, L. H.; Valverde, A. L.; Ribeiro, C. M. R.; de Albuquerque, A. C. F.; Carneiro, J. W. M.; Fiorot, R. G.; dos Santos Jr., F. M.; *New J. Chem.* **2020**, *44*, 8055. [Crossref]

119. Green, J. C.; Jiménez-Alonso, S.; Brown, E. R.; Pettus, T. R. R.; *Org. Lett.* **2011**, *20*, 5500. [Crossref]

120. Harrison, B.; Crews, P.; *J. Org. Chem.* **1997**, *8*, 2646. [Crossref]

121. Czajkowska-Szczykowska, D.; Jastrzebska, I.; Rode, J. E.; Morzycki, J. W.; *J. Nat. Prod.* **2019**, *82*, 59. [Crossref]

122. Lei, X.; Li, Y.; Lai, Y.; Hu, S.; Qi, C.; Wang, G.; Tang, Y.; *Angew. Chem., Int. Ed.* **2021**, *60*, 4221. [Crossref]

123. Terra, B. S.; Osorio, A. M. B.; de Oliveira, A.; Santos, R. P. M.; Mouro, A. P.; de Araújo, N. F.; da Silva, C. C.; Martins, F. T.; Vieira, L. B.; Bonaventura, D.; de Abreu, H. A.; Alcântara, A. F. C.; de Fátima, A.; *J. Braz. Chem. Soc.* **2017**, *28*, 2313. [Crossref]

124. da Silva, D. L.; Terra, B. S.; Lage, M. R.; Ruiz, A. L. T. G.; da Silva, C. C.; de Carvalho, J. E.; Carneiro, J. W. M.; Martins, F. T.; Fernandes, S. A.; de Fátima, A.; *Org. Biomol. Chem.* **2015**, *13*, 3280. [Crossref]

125. Kumar, A.; Sharma, S.; Maurya, R.; Sarkar, J.; *J. Comb. Chem.* **2010**, *12*, 20. [Crossref]

126. Naidu, K. R. M.; Krishna, B. S.; Kumar, M. A.; Arulselvan, P.; Khalivulla, S. I.; Lasekan, O.; *Molecules* **2012**, *6*, 7543. [Crossref]

127. Rama, V.; Kanagaraj, K.; Pitchumani, K.; *Tetrahedron Lett.* **2012**, *53*, 1018. [Crossref]

128. Zeikus, J. G.; Jain, M. K.; Elankovan, P.; *Appl. Microbiol. Biotechnol.* **1999**, *51*, 545. [Crossref]

129. Suresh; Saini, A.; Kumar, D.; Sandhu, J. S.; *Green Chem. Lett. Rev.* **2009**, *2*, 29. [Crossref]

130. Nakajima, M.; Adachi, Y.; Nemoto, T.; *Nat. Commun.* **2022**, *13*, 152. [Crossref]

131. Rodríguez-deLeón, E.; Jiménez-Halla, J. O. C.; Báez, J. E.; Bah, M. M.; *Molecules* **2019**, *24*, 1386. [Crossref]

132. Wu, J.-P.; Li, L.-Y.; Li, J.-R.; Yu, M.; Zhao, J.; Xu, Q.; Gu, Y.-C.; Zhang, T.; Zou, Z.; *J. Nat. Prod.* **2022**, *6*, 1522. [Crossref]

133. Zhang, B.; Wang, K. B.; Wang, W.; Wang, X.; Liu, F.; Zhu, J.; Shi, J.; Li, L. Y.; Han, H.; Xu, K.; Qiao, H. Y.; Zhang, X.; Jiao, R. H.; Houk, K. N.; Liang, Y.; Tan, R. X.; Ge, H. M.; *Nature* **2019**, *568*, 122. [Crossref]

134. Jackson, R. B.; Friedlingstein, P.; Andrew, R. M.; Canadell, J. G.; Le Quéré, C.; Peters, G. P.; *Environ. Res. Lett.* **2019**, *14*, 121001. [Crossref]

135. Wen, M.; Mori, K.; Kuwahara, Y.; An, T.; Yamashita, H.; *Appl. Catal., B* **2017**, *218*, 555. [Crossref]

135. Intergovernmental Panel on Climate Change (IPCC): *Climate Change 2022: Mitigation of Climate Change. Contribution of Working Group III to the Sixth Assessment Report of the Intergovernmental Panel on Climate Change*; Shukla, P. R.; Skea, J.; Slade, R.; Al Khourdajie, A.; van Diemen, R.; McCollum, D.; Pathak, M.; Some, S.; Vyas, P.; Fradera, R.; Belkacemi, M.; Hasija, A.; Lisboa, G.; Luz, S.; Mally, J., eds.; Cambridge University Press: Cambridge, UK and New York, USA, 2022. [Crossref] accessed in March 2023

136. IEA, *Key World Energy Statistics 2021*, https://www.iea.org/reports/key-world-energy-statistics-2021, accessed in March 2023.

137. dos Santos, T. C.; Ronconi, C. M.; *Rev. Virtual Quim.* **2014**, *6*, 112. [Crossref]

138. Saeed, I. M.; Alaba, P.; Mazari, S. A.; Basirun, W. J.; Lee, V. S.; Sabzoi, N.; *Int. J. Greenhouse Gas Control.* **2018**, *79*, 212. [Crossref]

139. dos Santos, T. C.; Lage, M. R.; da Silva, A. F. M.; Fernandes, T. S.; Carneiro, J. W. M.; Ronconi, C. M.; *J. CO2 Util.* **2022**, *61*, 102054. [Crossref]

140. Orestes, E.; Ronconi, C. M.; Carneiro, J. W. M.; *Phys. Chem. Chem. Phys.* **2014**, *16*, 17213. [Crossref]

141. Hu, X.; Liu, L.; Luo, X.; Xiao, G.; Shiko, E.; Zhang, R.; Fan, X.; Zhou, Y.; Liu, Y.; Zeng, Z.; Li, C.; *Appl. Energy* **2020**, *260*, 114244. [Crossref]

142. Duan, H.; Zhu, K.; Lu, H.; Liu, C.; Wu, K.; Liu, Y.; Liang, B.; *Chin. J. Chem. Eng.* **2020**, *28*, 104. [Crossref]

143. Zhu, X.; Lu, H.; Wu, K.; Zhu, Y.; Liu, Y.; Liu, C.; Liang, B.; *Environ. Sci. Technol.* **2020**, *54*, 7570. [Crossref]

144. Furtado, I. O.; dos Santos, T. C.; Vasconcelos, L. F.; Costa, L. T.; Fiorot, R. G.; Ronconi, C. M.; Carneiro, J. W. M.; *Chem. Eng. J.* **2021**, *408*, 128002. [Crossref]

145. García, J. I.; García-Marín, H.; Pires, E.; *Green Chem.* **2014**, *16*, 1007. [Crossref]

146. IEA, *Carbon Capture, Utilisation and Storage (CCUS) is a Unique Low-Carbon Solution which Significantly Reduces CO2 Emissions from Across the Economy*, https://www.ccsassociation.org/discover-ccus/explore-ccus/, accessed in March 2023.

147. Miranda, J. L.; de Moura, L. C.; Ferreira, H.; de Abreu, T. P.; *Rev. Virtual Quim.* **2018**, *10*, 1915. [Crossref]

148. Dabral, S.; Schaub, T.; *Adv. Synth. Catal.* **2019**, *361*, 223. [Crossref]

149. Dibenedetto, A.; Angelini, A.; *Adv. Inorg. Chem.* **2014**, *66*, 25. [Crossref]

150. Sakakura, T.; Kohno, K.; *Chem. Commun.* **2009**, *11*, 1312. [Crossref]

151. de Andrade, K. N.; da Costa, L. M.; Carneiro, J. W. M.; *J. Phys. Chem. A* **2021**, *125*, 2413. [Crossref]

152. Aresta, M.; Dibenedetto, A.; Angelini, A.; Pápai, I.; *Top. Catal.* **2015**, *58*, 2. [Crossref]

153. Ballivet-Tkatchenko, D.; Burgat, R.; Chambrey, S.; Plasseraud, L.; Richard, P.; *J. Organomet. Chem.* **2006**, *691*, 1498. [Crossref]

154. Choi, J.; Sakakura, T.; Sako, T.; *J. Am. Chem. Soc.* **1999**, *121*, 3793. [Crossref]

155. Moldowan, J. M.; Seifert, W. K.; Gallegos, E. J.; *AAPG Bull.* **1985**, *69*, 1255. [Crossref]

156. Pudi, A.; Rezaei, M.; Signorini, V.; Andersson, M. P.; Baschetti, M. G.; Mansouri, S. S.; *Sep. Purif. Technol.* **2022**, *298*, 121448. [Crossref]

157. Agbroko, O. W.; Piler, K.; Benson, T. J.; *ChemBioEng Rev.* **2017**, *4*, 339. [Crossref]

158. Shah, M. S.; Tsapatsis, M.; Siepmann, J. I.; *Chem. Rev.* **2018**, *118*, 2297. [Crossref]

159. Fiorot, R. G.; Carneiro, J. W. M.; *Tetrahedron* **2020**, *76*, 131112. [Crossref]

160. Liu, N.; Huang, W.; Tang, M.; Yin, C.; Gao, B.; Li, Z.; Tang, L.; Lei, J.; Cui, L.; Zhang, X.; *Chem. Eng. J.* **2019**, *359*, 254. [Crossref]

161. Zhang, S.; Liu, Y.; Gu, P.; Ma, R.; Wen, T.; Zhao, G.; Li, L.; Ai, Y.; Hu, C.; Wang, X.; *Appl. Catal., B* **2019**, *248*, 1. [Crossref]

162. Xiong, T.; Cen, W.; Zhang, Y.; Dong, F.; *ACS Catal.* **2016**, *6*, 2462. [Crossref]

163. Rong, X.; Qiu, F.; Rong, J.; Zhu, X.; Yan, J.; Yang. D.; *Mater. Lett.* **2016**, *164*, 127. [Crossref]

164. Orrego-Hernández, J.; Dreos, A.; Moth-Poulsen, K.; *Acc. Chem. Res.* **2020**, *8*, 1478. [Crossref]

165. Kolpak, A. M.; Grossman, J. C.; *Nano Lett.* **2011**, *11*, 3156. [Crossref]

166. Mansø, M.; Tebikachew, B. E.; Moth-Poulsen, K.; Nielsen, M. B.; *Org. Biomol. Chem.* **2018**, *16*, 5585. [Crossref]

167. Wang, Z.; Roffey, A.; Losantos, R.; Lennartson, A.; Jevric, M.; Petersen, A. U.; Quant, M.; Dreos, A.; Wen, X.; Sampedro, D.; Börjesson, K.; Moth-Poulsen, K.; *Energy Environ. Sci.* **2019**, *12*, 187. [Crossref]

168. Quant, M.; Hillers-Bendtsen, A. E.; Ghasemi, S.; Erdelyi, M.; Wang, Z.; Muhammad, L. M.; Kann, N.; Mikkelsen, K. V.; Moth-Poulsen, K.; *Chem. Sci.* **2022**, *3*, 834. [Crossref]

169. Houk, K. N.; Liu, F.; *Acc. Chem. Res.* **2017**, *50*, 539. [Crossref]